

Adaptive design of experiments methodology for noise resistance with unreplicated experiments

Lucas Caparini^a, Gwynn J. Elfring^a, Mauricio Ponga^{a,*}

^a*Department of Mechanical Engineering, 2054-6250 Applied Science Lane, Vancouver BC, Canada, V6T 1Z4*

Abstract

A new gradient-based adaptive sampling method is proposed for design of experiments applications which balances space filling, local refinement, and error minimization objectives while reducing reliance on delicate tuning parameters. High order local maximum entropy approximants are used for metamodelling, which take advantage of boundary-corrected kernel density estimation to increase accuracy and robustness on highly clumped datasets, as well as conferring the resulting metamodel with some robustness against data noise in the common case of unreplicated experiments. Two-dimensional test cases are analyzed against full factorial and latin hypercube designs and compare favourably. The proposed method is then applied in a unique manner to the problem of adaptive spatial resolution in time-varying non-linear functions, opening up the possibility to adapt the method to solve partial differential equations.

Keywords: adaptive sampling, radial basis functions, kernel density estimation, interpolation, max-ent, response surface modelling, sequential sampling, HOLMES, design of experiments, leave-one-out error

1. Introduction

Practical design problems often involve adjusting multiple parameters and understanding how each parameter influences quantities of interest. These quantities essentially are functions of multiple variables and often display complicated behaviour. Generally, it is not realistic to model such functions analytically, so numerous experiments, often numerical, are conducted to collect data and construct a simplified metamodel, from which further design decisions can be made.

Design of experiments (DoE) techniques have been developed to create an optimal metamodel from affordable data points and are broadly categorized into adaptive and non-adaptive techniques. Non-adaptive methods seek to increase the accuracy of the metamodel by placing samples in a statistically optimal manner throughout the parameter space [1] without using any additional information gained from previous sample points [2]. Once all desired points in the design space have been selected the data may be fit with any appropriate metamodel. Common examples include full factorial designs (FF), latin hypercube (LH) sampling [3], and orthogonal arrays [4]. A large family of non-adaptive methods treat data point selection as a large-scale optimization problem with an objective function chosen to maximize information entropy [5, 6, 7]. The maximum-entropy (max-ent) approach has gained popularity because it minimally biases the metamodel, and provides greater resistance to measurement error, but

*Corresponding author

suffers computationally from being combinatorial in nature. Thus, the many gradual advances in this approach have seen the non-deterministic polynomial-time-hard combinatorial optimization problem, which is generally not solvable in polynomial time, steadily become tractable for larger problems [8, 1, 9]. Other modern advances include features such as Bayesian frameworks for increased performance on highly nonlinear functions [10], handling of missing feature data [11], and the incorporation of sparsity-promoting heuristics, such as found in compressed sensing [12, 13, 14]. Nonetheless, the vast majority of non-adaptive methods essentially result in a space-filling distribution of data points through the design space.

Previous works have elucidated some potential benefits of non-space-filling designs from a statistical perspective [15], validating the intuition that some areas may need more refinement than others. Adaptive DoE methods utilize information from previous data points to recommend future test points, theoretically allowing targeted refinement in areas where the metamodel poorly approximates the underlying function. Early efforts were not met with consistent success [2], but that situation has been steadily improving. While some effort has been made to reconcile the maximum-entropy family with fully adaptive design [16], many recent efforts use common engineering heuristics instead of a rigid statistical approach, and have shown impressive performance compared to space-filling methods on test problems [17, 18, 19]. Recent developments have further extended and improved these techniques by incorporating data-dependent smoothing parameters, which improved results over noisy experimental data [19]. Those adaptive methods which remain dominantly statistical will generally use some approximation of metamodel error in the adaptivity scheme [20]. Recent works have particularly affirmed the usefulness of leave-one-out (LOO) cross-validation error in adaptive DoE [21, 22]. At this point adaptive approaches have progressed to demonstrate success on both analytical test problems and practical applications, such as chemical engineering [23] and aerodynamics [24].

Unlike non-adaptive methods, in adaptive DoE methods the metamodel is an important component of the technique itself. Nearly all modern DoE techniques must create metamodels over unstructured multidimensional data. The number of unstructured multidimensional interpolation techniques available is relatively small despite active research in the field for many years [25, 26]. Nearest-neighbor interpolation and inverse distance weighting are easy to implement but have obvious and well-known drawbacks. Mesh generation difficulties limit popular engineering techniques such as finite element shape functions even in three dimensions [27], let alone arbitrary dimensions. Moving least squares and Radial Basis Functions (RBF) require solving a costly system of equations and are relatively parameter-sensitive [28]. Gaussian process regression, also known as Kriging, is extremely popular among statistically-based adaptive DoE methods [29, 23, 20], but has similar parameter sensitivity. The local maximum-entropy (LME) functions [30] are a relatively new class of approximants designed specifically for solving PDEs with an unstructured multidimensional discretization [31, 32], and using only a single easily tuned parameter. While they have seen much attention in the realm of meshfree PDE simulation [33, 34, 35], little notice has been taken outside of that field. Extensions of the basic LME formulation have resulted in a family of related approximants [36, 37] of which the Higher-Order LME Scheme (HOLMES) [38] is used in this

work.

The accuracy of the metamodel, and thus any adaptive DoE technique, depends on the reliability of the data provided to it. Multiple data points at the same position in the design space can help alleviate this concern by providing some statistical bounds on the data values which can generate data-dependent smoothing parameters for the metamodel [19]. Unfortunately, even as sampling techniques and efficiency increase, practical constraints frequently require the use of unreplicated data points from which no statistical features may be inferred [39]. The experimentalist is then forced to retreat to the delicate task of manually tuning metamodel smoothing parameters or forego them entirely and use an exact interpolant.

This paper aims to take advantage of the natural error resistance of HOLMES approximants to create an adaptive DoE method that provides error resistance without depending on multiple sensitive smoothing parameters. The manuscript is organized as follows: The adaptive DoE algorithm is described in section 2. Construction and use of HOLMES approximants in the metamodel is addressed in section 3, and a simple kernel density estimation algorithm is proposed for automatically determining the local node spacing. The influence of the metamodel kernel parameter on the novel DoE method is evaluated in section 4, and the performance of the completed DoE algorithm is evaluated on a variety of analytical solutions. Finally, subsection 4.4 sees the DoE method applied beyond the realm of experimental design, and used to dynamically increase resolution of time-evolving functions.

2. Adaptive Design of Experiments Scheme

Most DoE algorithms maximize or minimize some objective function when selecting new data points. Adaptive methods differ from non-adaptive by utilizing the metamodel within the objective function, allowing the model to become iterative. This section details a specific choice of objective function (subsection 2.1) and associated iterative DoE algorithm (subsection 2.2). Details about the metamodel are left to section 3.

2.1. Objective Function

Assume a design space $\Omega \subseteq \mathbb{R}^d$, and an unknown function, $u : \Omega \rightarrow \mathbb{R}$, which may be evaluated through either computer or physical experiments. Furthermore, assume $u(x)$ has already been evaluated at some points $x_a \in \Omega$ called nodes, or data points. These values have been used to create a metamodel, $u_I(x; x_a) : \Omega \rightarrow \mathbb{R}$ which approximates u .

A scalar objective function, $S(x) : \Omega \rightarrow \mathbb{R}$, is desired which can be maximized to find the next data point for experimental evaluation via

$$x_{a+1} = \arg \max_{x \in \Omega} S(x). \quad (1)$$

Several heuristics and practical constraints are here used to determine the form of $S(x)$. Assuming other factors are equal, one such heuristic stipulates that proposed points should be placed in a space-filling manner throughout the domain. The associated constraint prevents duplicate selection of data points. Similarly, areas of low metamodel accuracy – where u_I approximates u poorly – should garner

more attention, while those with perfect accuracy should not be suggested. A final heuristic follows the common intuition that areas of a domain where u is highly nonlinear require more data points to be well captured by u_I and deserve more attention. Therefore, we propose the following heuristic objective function in a simple separable form,

$$S(x) = Q_L Q_S Q_E. \quad (2)$$

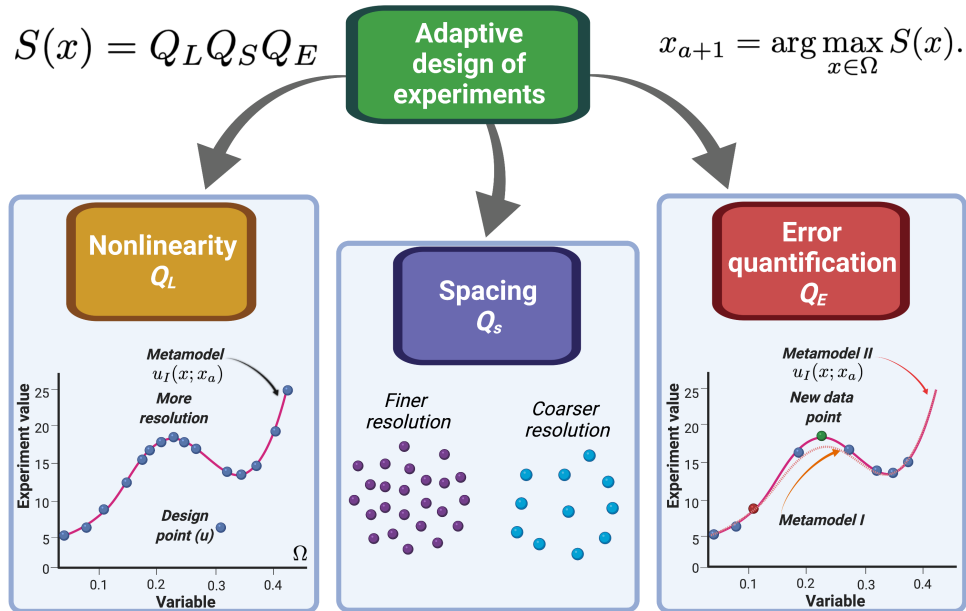


Figure 1: Schematic representation of the adaptive design of experiment objective function proposed in this work. Three fundamental parts, namely, nonlinearity, spacing and error are key descriptors used in the heuristic approach.

Figure 1 shows schematically the three different heuristics taken in our work. The objective function in (2) is composed of three multiplicative factors: Q_L representing the contribution of nonlinearities, Q_S the point spacing heuristic, and Q_E the metamodel error. Each factor is normalized onto the range $[\epsilon, 1]$, where $\epsilon = 10^{-4}$ to prevent difficulties when one of the factors becomes zero, or very close to zero, throughout the parameter space. In that case the resulting point placements would become dominated by numerical error, rather than the remaining factors. In this case $S(x) : \Omega \rightarrow [\epsilon^3, 1]$.

The product form of $S(x)$ is chosen to satisfy constraints associated with each heuristic by making $S(x)$ small when the constraint is violated. For instance, if no metamodel error is observed in some area of the domain there is very little reason to place points in that region, so the the objective function should assume a low value regardless of the other factors. Similar arguments can be made for the linearity and spacing components of the objective function. If a component of the objective function needs to be weighted more than the others, its exponent can be altered, though the effects of this were not heavily investigated in this work, and instead each component is treated as equally important. The objective function proposed here is similar to other works [17, 18, 19] in that a set of intuitive engineering heuristics are used to select future data points. This form additionally avoids the combinatorially large optimization problem involved with compressed sensing [40], or non-adaptive max-ent DoE methods [41]. Each of the three factors is now expanded upon in detail.

2.1.1. Nonlinearity, Q_L

The nonlinearity of the function, u , is emphasized in the objective function, S , based on the assumption that highly nonlinear areas will be approximated more poorly than linear areas (see Figure 1, left panel). The contribution is quantified by the magnitude of the Laplacian of the metamodel,

$$s = |\nabla^2 u_I(x)|, \quad (3)$$

which is a convenient choice as an invariant of the Hessian matrix. This choice consciously prioritizes maxima and minima of functions, and would not be ideal in the case of a perfect saddle point. If such a scenario was expected from the preliminary data, it would be simple to adjust this criterion to use the sum of the magnitudes of the diagonal components of the Hessian, or some other simple metric. No significant changes were found in this work with the examples selected, so the magnitude of the Laplacian is used through the remainder of this work.

To achieve consistent results with various functions, the Laplacian is normalized onto the range $[\epsilon, 1]$ via

$$s_n(x) = \frac{s(x) - \min_{x \in \Omega} s(x)}{\max_{x \in \Omega} s(x) - \min_{x \in \Omega} s(x)} (1 - \epsilon) + \epsilon. \quad (4)$$

Any quantity similarly normalized will be denoted $(\cdot)_n$ throughout the remainder of this work. Since (4) only works when the optimization is performed via an exhaustive search over Ω , providing explicit values of $\min_{x \in \Omega}$ and $\max_{x \in \Omega}$. Other optimization techniques for $S(x)$ must slightly alter this approach. Normalizations such as (4) are performed using maximum and minimum values from a previous iteration of the metamodel, and are observed to achieve similar results in the examples investigated here. Values of $s_n(x)$ approaching computer precision are automatically rounded to zero to enforce consistent behavior of the algorithm.

The linearity factor, Q_L , requires an interpolation method to approximate second-order derivatives over scattered data. Q_L must be updated along with the metamodel and is selected to simply be the normalized Laplacian,

$$Q_L = s_n. \quad (5)$$

2.1.2. Spacing, Q_S

The spacing factor discourages clumping and prevents duplication of data points (see Figure 1, central panel). The creation of a suitable spacing factor was investigated thoroughly before [17] and the form

$$Q_S = (1 - H(x))^2 \quad (6)$$

was decided upon after several tests.

Here, the spacing function $H(x)$ takes values of one at known data points and zero far away from data points. Mackman *et al.* [17] created a smooth $H(x)$ custom to the data set using Gaussian RBF interpolation with no appended polynomial constraints. The custom spacing function is then a simple interpolation function using Gaussian functions centered at each node, as in

$$H(x) = \sum_{a=1}^{N_a} \nu_a e^{-\xi \|x - x_a\|^2}. \quad (7)$$

Weights for each data point are obtained by solving the linear system

$$\sum_{j=1}^{N_a} \Phi_{ij} \nu_j = 1,$$

in which N_a is the number of nodes, ν is the unknown vector of weights, and the matrix is defined as $\Phi_{ij} = e^{-\xi \|x - x_a\|^2}$ for $i, j = 1, 2, \dots, N_a$.

Note that Q_S must be updated after each point is proposed in order to prevent point duplication.

The use of Gaussian RBFs requires the user to select a kernel parameter, ξ . This *ad-hoc* selection has a significant influence on the resulting points distribution and efficacy of the approach. The kernel parameter is selected based on a desired support radius, R_{supp} , and numerical tolerance, tol ,

$$\xi = -\log(tol) / R_{\text{supp}}^2. \quad (8)$$

Previous works [17, 19] achieved consistent results by selecting the desired support radius as a multiple of the fill distance, d_{fill} , which is the largest nearest-neighbor distance:

$$R_{\text{supp}} = R_0 \left(\frac{1}{2} d_{\text{fill}} \right). \quad (9)$$

Here R_0 is the scalar parameter and d_{fill} is the fill distance given by

$$d_{\text{fill}} = \sup_{x \in \Omega} \min_{x_a \in \mathcal{X}} \|x - x_a\|. \quad (10)$$

where \mathcal{X} is the set of all nodes. The sensitivity of the algorithm to the parameter R_0 and suggestions for selection are detailed in subsection 4.2.

2.1.3. Error Quantification, Q_E

Leave-one-out cross-validation error (LOO) is well known within the statistical community for its superior error estimation abilities [42]. Its inclusion has significantly increased the performance of adaptive DoE methods in the past [22]. LOO quantifies how much the addition of a data point to the model has increased the model's accuracy by comparing metamodel performance without the data to the known value. To evaluate LOO at the known data point x^* , where $u(x^*)$ is known, a metamodel is constructed excluding this point, $u_I^*(x)$. The LOO error is then given by comparison of $u_I^*(x)$ with $u(x)$ at x^* :

$$\epsilon_{\text{LOO}}(x^*) = |u(x^*) - u_I^*(x^*)|. \quad (11)$$

A point whose addition significantly influences the metamodel will garner a large LOO value. Additional sampling is likely needed in that vicinity, since the metamodel is now known to have been capturing it poorly. This idea is schematically illustrated in Figure 1, right panel. The red point adds little improvement to the metamodel while the green one critically improves the metamodel. Therefore, the adaptive DoE technique should be biased to further explore the area around the green point.

In our implementation, LOO errors at every data point are evaluated and subsequently normalized to the range $[\epsilon, 1]$, with values approaching computer precision receiving a value of zero automatically.

While LOO error can only be evaluated at known data points, Q_E must be evaluated at any location in the design space, which is accomplished by interpolation of LOO values. Here, the same interpolation

method used for the metamodel is used for LOO error, with the implied assumption that $\epsilon(x)_{\text{LOO},n} : \Omega \rightarrow [\epsilon, 1]$ is a smooth function in space. Under this assumption, then we can evaluate Q_E as

$$Q_E(x) = \epsilon_{\text{LOO},n}(x) = \sum_{i=1}^{N_a} w_a(x) \epsilon_{\text{LOO},n}(x_a), \quad (12)$$

where w_a are the shape functions associated with the nodes x_a . Since Q_E relies on explicit interpolation of known data points, it is updated with the metamodel.

Evaluating LOO error requires reconstructing the metamodel at each node location for the evaluation of $u_I^*(x^*)$. If the metamodel is challenging to construct or the dataset is large, this step can become costly. The metamodel described in section 3 performs single point evaluations quite quickly, so it is not significantly penalized by using LOO. The RBF metamodel used by others [17] is not a reasonable choice as a metamodel in this scenario because of the high computational cost of metamodel construction which would be required with each $u_I^*(x^*)$ evaluation.

Like with the linearity factor, Q_L , the LOO criterion, Q_E , cannot be reevaluated until new experimental data is collected. This allows multiple points to be suggested at once by the algorithm without the computational cost of LOO evaluation. Furthermore, additional data points only require LOO to be reevaluated in the area immediately surrounding them, rather than for the entire domain. This is described further in 2.2 below.

2.2. Point Selection Algorithm

A single data point may be found through equation (1); however, most experimentalists will prefer receiving multiple data point recommendations simultaneously to take advantage of batch processing. The proposed DoE algorithm can recommend multiple distinct data points to the experimentalist, provided Q_S is updated appropriately.

Suppose an experimentalist can gather N_p data points per day, and would like to use the DoE algorithm to propose the next data points to gather within the design space. There are N_{iter} days allotted for collecting data, and a starting data set of x_0 data points and the corresponding results of $u_0 = u(x_0)$. The resulting DoE and experimental workflow would look as in algorithm 1. Each day the new data points would be used to construct a new metamodel, from which Q_L and Q_E are derived. From there N_p unique points are proposed by alternately evaluating (1) and updating Q_S to include the point already suggested. After all N_p points have been recommended, the experimentalist can add them to the dataset.

The described algorithm is necessary to recommend multiple points at once because Q_S must be updated to prevent the same point being recommended every time. Because Q_S is not dependent on the experimental results, but only the position of previous points within the design space, it is perfectly acceptable to update it without new experimental results. Similarly, neither Q_L nor Q_E can be adjusted until new experimental data is available. There is no need to recompute them, and some computational power can be saved.

Q_L and Q_E cannot be updated when multiple points are proposed, but only whenever new experimental values are learned and the metamodel is updated. This suggests a two-tiered update mechanism

for the DoE algorithm. An inner loop will propose N_p new data points by updating Q_S at every iteration. An outer loop takes the proposed points, evaluates them through experiments, updates the metamodel and associated Q_L and Q_E values, and finally passes everything back to inner loop to get more points. The outer loop operates for a specified amount of iterations, N_{iter} , while would usually correlate to a predetermined number of data points or metamodel accuracy.

Algorithm 1 Adaptive DoE Procedure

```

1: Create initial data points,  $x_0$ .
2: Evaluate  $u_0 = u(x_0)$ .
3: for  $i = 1, \dots, N_{\text{iter}}$  do
4:   Create interpolation scheme,  $u_I(x) = \sum_a w_a(x)u_{0,a}$ .
5:   Evaluate and normalize LOO error at data points,  $\epsilon_{\text{LOO},n}$ .
6:   Interpolate  $Q_L$  and  $Q_E$  onto test points in domain.
7:   for  $j = 1 \dots N_p$  do
8:     Create spacing function,  $H(x_0, x_{\text{new}})$ .
9:     Interpolate  $Q_S$  onto test points in domain.
10:    Select new optimum,  $x_{\text{new},j} = \arg \max S(x)$ , through any optimization method.
11:  end for
12:  Evaluate  $u_{\text{new}} = u(x_{\text{new}})$ .
13:  Concatenate Data,  $x_0 \leftarrow [x_0; x_{\text{new}}]$ ,  $u_0 \leftarrow [u_0; u_{\text{new}}]$ .
14: end for

```

The solution of equation (1) required for each iteration of the inner loop could be done in any convenient method. Every example in this work has performed an exhaustive search over a finely discretized domain. More advanced methods will require small modifications to the normalizations used in Q_L and Q_E , as discussed in 2.1.1.

3. HOLMES Metamodel

Evaluating the nonlinearity parameter (5) requires a metamodel capable of approximating the Hessian of $u(x)$. The HOLMES approximants developed by Bompadre *et al.* [38] are used here rather than the more common RBF, or polyharmonic spline (PHS) interpolation methods. HOLMES is based on the LME shape functions [30] and ultimately the max-ent functions previously introduced by Sukumar [43]. HOLMES is known to function in any dimension without alteration to its original formulation, and does not require structured input data. It also does not require the solution of a large system of equations during its evaluation. This section outlines the construction of HOLMES and modifications necessary for use in the adaptive DoE method.

3.1. Basic Implementation

The HOLMES consists in a set of shape, or basis, functions, $w_a(x)$, centered around a corresponding set of nodes, or data points, x_a , situated in the design space $\Omega \subseteq \mathbb{R}^d$. If the values of the unknown function, $u(x)$, are known at the nodes, HOLMES may be used to construct a metamodel in the same manner as any interpolation scheme,

$$u_I(x) = \sum_{x_a \in \mathcal{N}_a(x)} w_a(x)u(x_a). \quad (13)$$

Here, $\mathcal{N}_a(x)$ denotes the set of nodes within a neighborhood of the query point x .

The HOLMES shape functions are formulated by solving a nonlinear multi-objective optimization problem which seeks to maximize both information entropy and minimize shape function width. Additional constraints are added in the form of Lagrange multipliers to ensure n^{th} order polynomial consistency. Details of the derivation may be found in the original work [38].

The resulting functions are the sum of negative and positive exponential components,

$$w_a(x) = w_a^+(x) - w_a^-(x) \quad (14)$$

$$w_a^\pm(x) = \exp \left[-1 - h^{-p} \gamma \|x - x_a\|_p^p \mp \left(\sum_{\alpha \in \mathcal{A}_{d,n}} h^{-|\alpha|} \lambda_\alpha (x - x_a)^\alpha \right) \right]. \quad (15)$$

The exponents are each composed of a simple decay term and an additional term which utilizes a Lagrange multiplier, λ , to explicitly enforce polynomial consistency of order n on the interpolant. The decay term, $-h^{-p} \gamma \|x - x_a\|_p^p$ uses a non-dimensional parameter, γ , the p -norm of distance, $\|\cdot\|_p$, and a measure of the nodal spacing, h , to determine the width of the shape function.

The third term in the argument of (15) is centered on the Lagrange multiplier, λ_α . This term uses the same h value as in the decay term to scale the Lagrange multiplier to roughly $\mathcal{O}(1)$ for faster convergence. Multi-index notation is used to concisely write out the polynomial component terms. In this notation, $\alpha \in \mathbb{N}^d$ is a multi-index used to represent each monomial component of an n^{th} order polynomial in \mathbb{R}^d . For instance, in three dimensions if $x = [\mu_1 \ \mu_2 \ \mu_3]$ and $\alpha = [1 \ 2 \ 1]$, then the notation $x^\alpha = \mu_1 \mu_2^2 \mu_3$. $\mathcal{A}_{d,n}$ is then the set of all valid multi-indexes combinations of dimension d and order less than or equal to n . The Lagrange multiplier, λ , is a vector whose length corresponds to the number of monomial components in a polynomial of the specified order and dimension, which can be easily found with the binomial coefficient function, $D_{d,n} = \binom{d+n}{n}$.

3.1.1. Regularized Newton Iterations

The Lagrange multipliers must be found implicitly as the solution to a nonlinear convex minimization problem, i.e.,

$$\lambda^*(x) = \arg \min_{\lambda \in \mathbb{R}^{D_{d,n}}} Z(x, \lambda), \quad (16)$$

$$Z(x, \lambda) = \lambda_0 + \sum_{a=1}^{N_a} [w_a^+(x, \lambda) + w_a^-(x, \lambda)]. \quad (17)$$

The problem given by (16) can be solved through Newton-Raphson iterations with explicit formulas provided by Bompadre *et al.* [38] and summarized in (18) through (20). Here the vector \mathbf{r} is the gradient of Z with respect to λ , and the matrix \mathbf{J} is the Hessian with respect to λ . The multiindices $\alpha, \beta \in \mathcal{A}_{d,n}$

correspond to specific components of the Lagrange multiplier vector, which is indexed by them.

$$r_0(x, \lambda) = \frac{\partial Z(x, \lambda)}{\partial \lambda_0} = 1 - \sum_{a=1}^{N_a} (w_a^+(x, \lambda) - w_a^-(x, \lambda)), \quad (18)$$

$$r_\alpha(x, \lambda) = \frac{\partial Z(x, \lambda)}{\partial \lambda_\alpha} = -h^{-|\alpha|} \sum_{a=1}^{N_a} (w_a^+(x, \lambda) - w_a^-(x, \lambda)) (x - x_a)^\alpha, \quad (19)$$

$$J_{\alpha\beta} = \frac{\partial^2 Z(x, \lambda)}{\partial \lambda_\alpha \partial \lambda_\beta} = h^{-(|\alpha|+|\beta|)} \sum_{a=1}^{N_a} (w_a^+(x, \lambda) + w_a^-(x, \lambda)) (x - x_a)^{\alpha+\beta}. \quad (20)$$

In practice, the Hessian matrix, \mathbf{J} , is often poorly conditioned – an effect which becomes worse as n or d increase. This issue imposes a practical limit to the order and dimension of HOLMES evaluations.

For the purposes of the present work, a regularization proposed by Polyak [44] suitably resolves this issue. It is implemented via a modification of the partition function, $Z(x, \lambda)$, into $\hat{Z}(x, \lambda, \Lambda)$, as seen in (21) to (24). This is a convenient modification because when the partition function and its derivatives are evaluated at $\Lambda = \lambda$ it returns the original partition function and gradient. The only values effected are the diagonal elements of the Hessian, to which the norm of the gradient is added.

$$\hat{Z}(x, \lambda, \Lambda) = Z(x, \Lambda) + \frac{1}{2} \|\nabla Z(x, \lambda)\| \|\Lambda - \lambda\|^2, \quad (21)$$

$$\hat{Z}(x, \lambda, \Lambda)|_{\Lambda=\lambda} = Z(x, \lambda), \quad (22)$$

$$\frac{\partial \hat{Z}(x, \lambda, \Lambda)}{\partial \Lambda}|_{\Lambda=\lambda} = \mathbf{r}(x, \lambda), \quad (23)$$

$$\frac{\partial^2 \hat{Z}(x, \lambda, \Lambda)}{\partial \Lambda_\alpha \partial \Lambda_\beta}|_{\Lambda=\lambda} = \mathbf{J}(x, \lambda) + \|\mathbf{r}(x, \lambda)\| \mathbf{I}. \quad (24)$$

The regularization above proved robust in all examples, but convergence issues appear again as d and n increase. Combining Newton’s method with an alternate optimization algorithm, such as Nelder-Mead or preconditioned conjugate gradient has been used to overcome similar difficulties with the related LME shape functions [45, 46] but were not pursued here. Instead, effort was placed in adjusting the kernel width to better suit the local node distribution and increase both robustness and accuracy. This is detailed in the next section.

3.2. Adjusting the Kernel Width

Any kernel-based interpolation scheme may face practical computational issues on real data sets. One such issue occurs when the data distribution is extremely uneven. Clumps of high density data occur in some places, while others are left relatively sparse. In theory, such clumped datasets would not cause an issue for HOLMES, but in reality it may lead to difficulty solving the convex optimization problem required for evaluating the Lagrange multipliers. Since any adaptive DoE approach will result in unevenly spaced datasets and potential clumping, it is worth investigating the effects an adjustable kernel parameter may have on HOLMES in terms of robustness and accuracy.

3.2.1. Nodal Spacing Parameter

Before any method of adjusting the kernel parameter can be introduced or evaluated, HOLMES must first be implemented in a manner that accepts variable kernel parameters. A similar operation has been

performed by for the related LME shape functions [47]. Though this is a small step, it is extremely important when considering situations where very large differences in spacing may be desirable. A constant kernel width is simply not feasible in such cases. Section 4 below will explore applications which could potentially result in such situations.

In equation (15) the kernel parameter is expressed by the term γh^{-p} , where γ is non-dimensional and h is a measure of the nodal spacing. Naïvely, h could be adjusted dynamically as a function of the query point location, $h(x)$, but this introduces additional terms into the HOLMES derivatives which are difficult to evaluate without an explicit formula for $h(x)$. Instead, the approach developed by Ref. [47] is taken. Instead of a single h value being used for all nodes, each node, x_a , is associated with its own h_a value. These h_a values must either be constant or determined in some other way which does not depend on the query point location in order to avoid generating more complicated derivative formulations for HOLMES.

This approach can be used with HOLMES provided one crucial observation: *Lagrange multipliers must only be a function of x* . The scaling term $h^{-|\alpha|}\lambda_\alpha$ only exists to speed convergence of Newton’s method and scale the elements of λ approximately onto the range $[0, 1]$. In this role, h has no actual influence on the final shape function. Allowing h to be a nodal parameter does not make sense inside this term and will ruin HOLMES convergence. The related LME literature never encountered such issues because, with the exception presented in Ref. [33] where adjustable h_a was not used, λ was never normalized by h . The nodal spacing parameter used for this scaling must now be distinct from the one used within the kernel parameter, and will be denoted h_g . It can be selected as the global average node spacing or as a function of position with a little care, but can never be a nodal parameter.

To further differentiate the node-dependent h value used in the kernel parameter, γh_a^{-p} , from the h value use to scale the Lagrange multipliers, h_g , the substitution $\beta_a = \gamma h_a^{-p}$ is made within the HOLMES shape functions. β_a represents the scaled, dimensional kernel parameter of node x_a , just as in the previous LME literature [47]. The new flavor of HOLMES is given by equation (25),

$$w_a^\pm(x) = \exp \left[-1 - \beta_a \|x - x_a\|_p^p \mp \left(\sum_{\alpha \in \mathcal{A}_{d,n}} h_g^{-|\alpha|} \lambda_\alpha (x - x_a)^\alpha \right) \right]. \quad (25)$$

Unlike the method used in Ref. [47], our modification does not substantially change the original derivative formulations, making the substitution quite convenient. Determination of the local average spacing is the subject of the next section.

3.2.2. Kernel Density Estimation

The spacing parameter h_a can now be chosen to reflect the local nodal spacing around a given point, rather than the global average. The approach we take is to approximate the local node density, $\rho(x)$ at a node, and deduce the local average spacing through

$$h(x) = \frac{1}{\rho(x)^{1/d}}, \quad (26)$$

since a density value is more intuitive than an average spacing value.

Kernel density estimation (KDE) has been used by the statistical community for many years to reconstruct an approximate probability density function from binned data [48]. KDE is a kernel convolution method with straightforward implementation and extensive literature [49]. To see how it is applied to non-binned point data in the form of nodal positions, consider convolving some density function, $\rho(x)$ with some kernel, $K(x)$, in order to obtain a smoothed approximation of the density function, $\hat{\rho}(x)$,

$$\hat{\rho}(x) = \int_{-\infty}^{\infty} \rho(x) \cdot K(x - y) dy. \quad (27)$$

If the kernel, $K(x)$, is chosen appropriately, it is known that this approximation becomes exact as the kernel width decreases to zero [49, 50]. However, the function $\rho(x)$ is not known beforehand except for at selected nodal points. Approximate the number density at each node by the global density over the domain, $\rho(x_a) \approx \rho_{avg} = N_a/V_\Omega$, and approximate the integral as

$$\hat{\rho}(x) \approx \rho_{avg} \sum_{a=1}^{N_a} K(x - x_a) \Delta V_a, \quad (28)$$

where, like the density at the nodes, the volume associated with each node is taken as the global average, $\Delta V_a = V_\Omega/N_a$. Since $\rho_{avg} \Delta V = 1$, the density estimate becomes a simple sum of kernel functions,

$$\hat{\rho}(x) \approx \sum_{a=1}^{N_a} K(x - x_a). \quad (29)$$

Thus, an estimate of node density can be evaluated at a point by a simple summation of kernel functions centered around adjacent nodes.

The simplicity and extensive history of KDE makes it an obvious choice for node density estimation. In fact, some LME works used a *local average* method to find $h(x_a)$,

$$h_a = \left(\frac{V_{k,a}}{k} \right)^{1/d}, \quad (30)$$

which can be viewed as KDE with a rectangular window kernel whose size adjusts to encompass k neighbours. Here $V_{k,a}$ is the volume of hypersphere encompassing k nodes around point x_a , and d is the spatial dimension.

A rectangular kernel will work well when the point density is nearly constant or changes slowly through the domain as shown in the left illustration in Figure 2, but will be poor when clustering exists, as in the right illustration in Figure 2. Instead, a more suitable choice of the kernel is to weight points in a smooth and monotonically decreasing manner from the node. Using a Gaussian function to approximate nodal density seems like the most obvious choice,

$$\hat{\rho}(x) \approx A \sum_{x_a \in \mathcal{N}_a(x)} \exp \left[-\frac{(\mathbf{x}_a - \mathbf{x}) \Sigma (\mathbf{x}_a - \mathbf{x})}{2} \right], \quad (31)$$

$$A = \frac{1}{\sqrt{(2\pi)^d |\Sigma|}}. \quad (32)$$

Here Σ is a matrix of decay parameters, which in this case is chosen to be diagonal such that $\Sigma_{ii} = \sigma_i^2$ for some vector $\sigma \in \mathbb{R}^d$. The constant A is chosen to normalize the integral. The Gaussian is a good choice

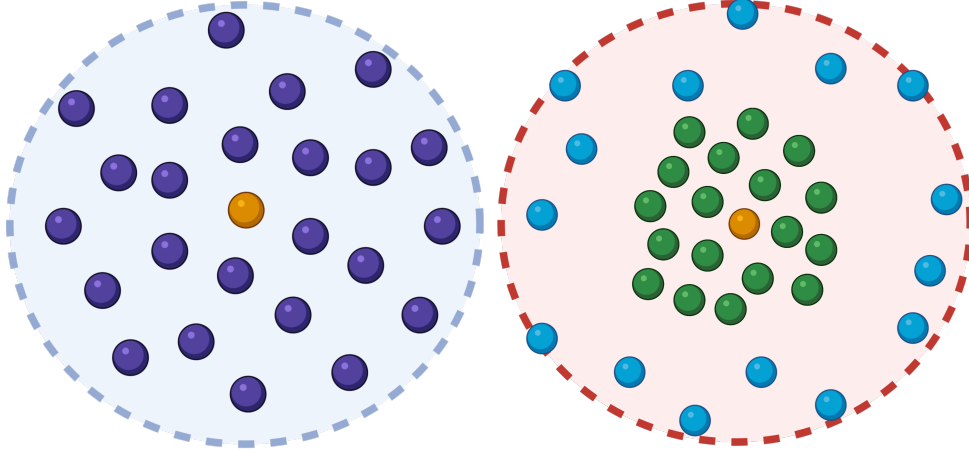


Figure 2: Smoothly changing point density *vs.* clustered data distribution. The points in the left figure are homogeneously distributed near the orange data point where as the green points shown in the right image are clustered around the orange ones. Moreover, the light blue points are placed further away from the orange point clearly indicating a change in the spatial resolution.

because it offers well-studied properties and takes few parameters, while also sporting much faster tail decay than simpler alternatives such as constant or linear kernels. Rapid tail decay is especially important for effective KDE estimation in higher dimensions [49]. It is also smoother than other popular options such as the Epanechnikov kernel [51]. Finally, while more specialized kernels often require a rapidly increasing number of parameters as the dimension increases, making them cumbersome for unsupervised tasks, the Gaussian kernel is trivial to apply to arbitrary dimensions.

The accuracy of KDE for this application is here assessed by comparison to a set of points placed at a known constant spacing. Let $\Omega = [0, 1]$ and an even nodal spacing of $h_a = 0.01$ be used to create a node-set within Ω . Figure 3a demonstrates the poor performance of the local averaging method ($k = 75$) when quantified in this manner, and better performance from the Gaussian convolution. The boundary bias is extreme in both cases as the kernels attempt to retrieve information where none should exist. The effect is stronger for the local averaging method because its zeroth-order kernel does not decay at the tails. The nodes in the middle of the domain do not suffer to the same extent because the individual kernels have decayed sufficiently prior to reaching the boundary.

Three steps are applied to correct the boundary errors: k -nearest neighbour (knn) windowing, volume correction, and automatic adaptivity of the Gaussian kernel parameter. The knn window function truncates the kernel to a boundary defined by the k^{th} nearest neighbour. The volume correction compensates for a kernel that is truncated at the edge of the convex hull of points. The kernel parameter adaptivity adjusts the kernel parameter according to how centered the query point is within its group of neighbours. The final effect of the boundary corrections is pictured in Figure 3b, where each of the analyzed kernels shown positioned on the domain boundary. While both the rectangular kernel and uncorrected Gaussian attempt to take information from outside the domain – information which does not exist – the corrected kernel is truncated at the boundary and changes its volume and width in a corresponding manner.

Limiting the integral approximation to only the nearest k neighbours means x_a need not be centered in Ω anymore, as long as it is near the center of the hypercube enclosing itself and its neighbours, $\Omega_{a,k}$. It

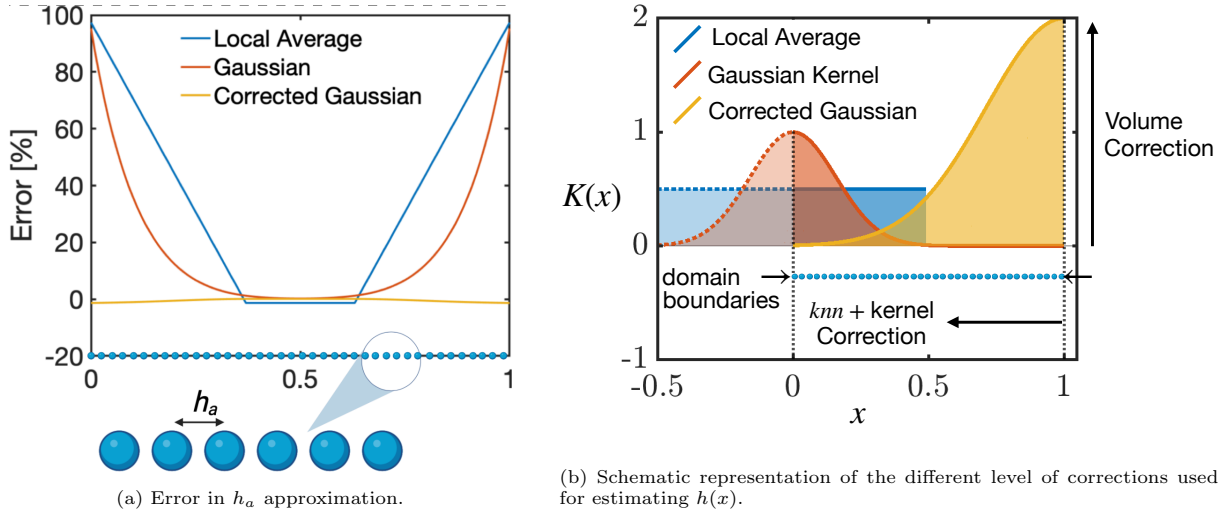


Figure 3: Behaviour of several boundary-corrected kernel density estimation method on 1D line with constant nodal spacing $h_a = 0.01$ using $k = 75$ nearest neighbours to estimate $h(x)$. (a) Error in h_a vs. x for local average (26), Gaussian (31) and three-step boundary correction procedure. (b) Schematic representation of the different approaches used for comparison. It is evident that the local average and Gaussian kernel try to retrieve information outside of the domain boundary where there is no data (the local average and Gaussian extend beyond the left boundary placed at $x = 0$). The corrected Gaussian approach rescales the Gaussian to avoid retrieving information outside the boundaries and thus, the Gaussian is rescaled.

also saves the computational cost of operating over the entire dataset. Since neighbouring is a practical necessity when operating over unstructured data, finding the first k neighbours should not be a significant additional computational burden.

A volume correction factor can then be applied,

$$\hat{\rho}'_a = \hat{\rho}_a \frac{V_{\mathbb{R}^d}}{V_{\Omega}}, \quad (33)$$

where

$$\frac{V_{\Omega}}{V_{\mathbb{R}^d}} = \left(\frac{1}{2}\right)^d \prod_{k=1}^d \left(\operatorname{erf}\left(\frac{\min |x_{a,d} - \partial\Omega_{a,k,d}|}{\sigma_d/\sqrt{2}}\right) + 1\right). \quad (34)$$

This recognizes that the convolution does not truly extend over \mathbb{R}^d , but $\Omega_{a,k}$. The previous normalization factor (32) is no longer appropriate. The volume correction factor approximately scales the density estimate to the correct value. The argument to the error function in (34) is the minimum distance from x_a to the boundary along each dimension d , $\partial\Omega_{a,k,d}$, scaled by σ_d . Truncation is only performed on the nearest boundary in each dimension in equation (34) because numerical results indicate a slight underestimate in point density is more beneficial than an overestimate. The total effect is to essentially rescale the convolution so it would integrate to unity on the reduced domain.

The final correction is to vary σ based on the proximity of x_a to $\partial\Omega_{a,k}$. It is optimal for the Gaussian kernel to decay sufficiently by the time it reaches the truncated portion of the domain, but without becoming so highly localized that the nodes chosen to be included do not contribute significantly to the estimate. Using

$$\sigma_i = \max |x_{a,i} - \partial\Omega_{a,i}|/N_{\sigma}, \quad (35)$$

with $N_{\sigma} \approx 3$ achieves an appropriate amount of decay. An interesting alternative to this approach would be to determine principal directions of the node distribution via PCA or SVD and select σ along those

directions in the manner of equation (35). The resulting Σ would generally not be diagonal after rotation. This option has not been considered here.

Finally, the nodal spacing may be approximated by inserting $\hat{\rho}'$ in place of $\rho(x)$ in equation (26),

$$h_a = \frac{1}{\hat{\rho}'(x_a)^{1/d}}$$

The result of each successive correction is seen in Figure 3b by comparison to nodes on $[0, 1]$ with spacing of $h_a = 0.01$. After all corrections are applied, the maximum error in this example is less than 1.5% on the boundary of the domain. Locations 10 nodes from the boundary are accurate to within 0.1% of the true value.

The final algorithm for h_a is given by Algorithm 2.

Algorithm 2 Adaptive nodal spacing parameter, h_a

- 1: **for** $x_a, a = 1, \dots, N_a$ **do**
 - 2: Find k nearest neighbours and determine the volume and boundaries of $\Omega_{a,k}$
 - 3: Solve for components of Σ using equation (35).
 - 4: Evaluate $\hat{\rho}(x_a)$ with equation (29).
 - 5: Evaluate $\hat{\rho}'$ with equation (33).
 - 6: Evaluate h_a using equation (26).
 - 7: **end for**
-

It should be noted that this approach to correcting boundary bias does not align perfectly with the standard KDE methodology. While using a window function to truncate the Gaussian kernel is common, the other two steps are variations chosen to operate sufficiently and conveniently without supervision. The volume correction factor resembles a folded distribution which is common in KDE [52, 53, 54]. Experiments using the same error quantification as Figure 3 revealed the folded normal distribution to perform similarly or slightly worse than the volume corrected normal distribution for this application (Figure 4). Since there is extra complexity involved in using a folded distribution in multiple dimensions [55], the simple volume correction is used instead. Similarly, algorithms have been developed for choosing kernel parameters – a variety of which are described in [49] – but these are often unnecessarily involved for a KDE scheme meant to operate cleanly as a background task. A similar argument can be made for using skewed distributions. They would likely be effective, but the extra difficulties involved in setting their parameters is unnecessary for this application. The simple boundary corrections proposed here are suitable for the context of this work.

3.2.3. HOLMES Accuracy with Adaptive h_a

Equipped with an adjusted HOLMES formulation and a method for varying the nodal spacing accurately, the effect of an adjustable kernel width on HOLMES interpolation accuracy can now be assessed.

Rastrigin’s function (Appendix A) is used for this analysis. The error in a HOLMES interpolation is quantified via the discrete ℓ_2 norm,

$$\ell_2 = \left[\sum_{p=1}^{N_p} (u(x_p) - u_I(x_p))^2 / N_p \right]^{1/2}. \quad (36)$$

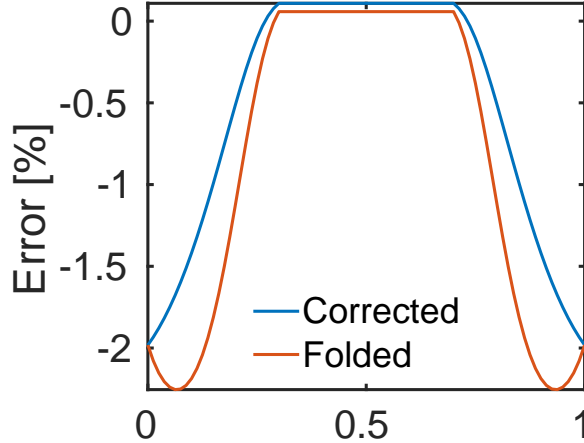


Figure 4: Error in the estimation of h_a in the interval $[0, 1]$ for a homogeneous distribution of size $h_a = 0.01$ as shown in Figure 3a. Proposed correction method *vs.* folded Gaussian [52, 53, 54] kernel density estimation obtained with $k = 50$ nearest neighbors and using a σ scaling factor of $N_\sigma = 2.9$ in the example.

In these tests x_p is a grid of 100×100 grid points covering the domain $[0, 1]^2$, which was found to produce consistent results. HOLMES functions were evaluated with parameters $p = 3$, order 3, and $\gamma = 0.12$.

Tests compared the performance of HOLMES when the kernel width was adapted in three separate ways: the KDE method proposed here using a modified Gaussian kernel, a simple KDE method using a rectangular kernel (an average of local values), and a non-adapted kernel where the global average of node spacing is used for all nodes. In all cases HOLMES was confirmed to converge at the appropriate rate as determined by its order of polynomial consistency.

To assess the performance of HOLMES and the h -approximation schemes on unevenly distributed, or *clumped* data the ℓ_2 error can be calculated over datasets with varying degrees of clumping. Clumping is quantified here by specifying a number of clumping centres around which data points are normally distributed. The standard deviation of the distribution is $1/4$ the distance between clumping centers. Figure 5a visualizes this. The accuracy of HOLMES can be plotted against the number of clumping centers, as seen in figure 5b.

The results of Figure 5b demonstrate a few things. Notably, the proposed adaptive method achieves better accuracy than either of the alternative approaches, and is more robust. When using a constant value for h_a HOLMES performs well if the nodes are more evenly distributed; however, accuracy drops below other approaches as the data becomes more uneven.

More concerning is the difficulty evaluating HOLMES in the highly clumped region using a constant global value for h_a . If the convex optimization problem required to determine the Lagrange multipliers can be solved within a reasonable number of Newton algorithm iterations – generally less than 20 – it is termed *robust*. If Newton’s method fails to converge, or takes an exceedingly long time to do so, such as more than 1000 iterations, it is not robust (and termed *poor*).

The rectangular kernel approach to adapting h_a is interesting in that it produces a less accurate HOLMES interpolation in general compared to both the proposed KDE method and the constant h method; however, it does generally remain fairly robust in the highly clumped tests, as desired.

The proposed KDE approach seems to perform the best with both even and uneven datasets, offering

a good balance of robustness and accuracy compared to the others. No method was able to be completely robust at the extremes of clumping with the parameters used in this test, as seen on the far left side of Figure 5b, where all methods have a dotted line, representing poor HOLMES robustness.

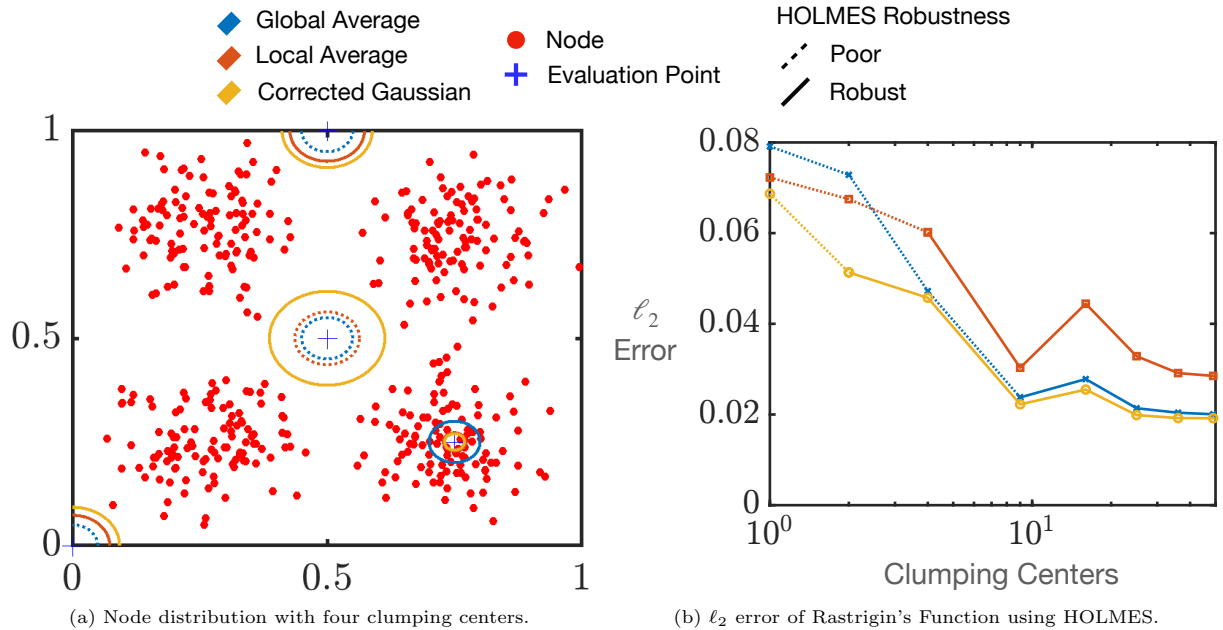


Figure 5: Performance comparison of the global average, local average (rectangular kernel) (26), and boundary corrected Gaussian (31) methods for assigning the spacing parameter, $h(x_a)$. (a) Spacing parameter estimated at different locations (indicated by a + marker) for a four cluster clumped data. (b) ℓ_2 norm error evolution as a function of the clumping centers for Rastrigin's function evaluated with the three different spacing parameter methods on a 100×100 grid points covering the domain $[0, 1]^2$. Continuous and dashed lines indicate robust and poor performance of the HOLMES metamodel using $p = 3$, order 3, and $\gamma = 0.12$.

3.3. Noise Resistance

A probability distribution which maximizes information entropy will have the greater resistance to errors caused by Gaussian white noise, which itself is the highest entropy form of noise [56]. HOLMES shape functions cannot be viewed as probability distributions because they lack a non-negativity constraint – a constraint necessarily lost in order to achieve higher orders of polynomial consistency [38, 36]; however, their formulation still depends on maximization of entropy, so they should exhibit resistance to Gaussian noise compared to most other shape functions.

Radial basis function interpolation is chosen to contrast HOLMES interpolation because of its huge popularity and use in other DoE applications. It is one of a few other methods which are effective at interpolating Hessian information over unstructured multidimensional data; however, in the forms analyzed, RBF interpolation performs worse than HOLMES when the data contains noise.

$$f_N(x) = f(x)(1 + \zeta G) \quad (37)$$

$$f_N(x) = f(x) + \zeta \max_{x \in [0, 1]^2} (f(x))G \quad (38)$$

HOLMES and RBF interpolation are compared in two related, but distinct scenarios which an experimentalist may encounter: pure white Gaussian noise, which injects normally distributed noise into the

data, and proportional Gaussian noise, which depends on the amplitude of the underlying signal. These are represented by (37) and (38) respectively. Here G is a Gaussian noise generator with a mean of 0 and standard deviation of 1, and ζ scales the amplitude of the noise. The first case of constant variance noise could occur when measurements are limited purely by the accuracy of the experimental apparatus. The second case could arise when experimental physics incite additional errors.

In both scenarios a standard convergence analysis on a regular grid can be carried out using a known function – Branin’s function is used here (Appendix A) – and the convergence of HOLMES and RBF interpolations compared as the noise magnitude is adjusted. In all tests the ℓ_2 error is plotted as a function of grid size. The ℓ_2 norm is evaluated using a 100×100 grid evenly spaced over the function domain $\Omega = [0, 1]^2$.

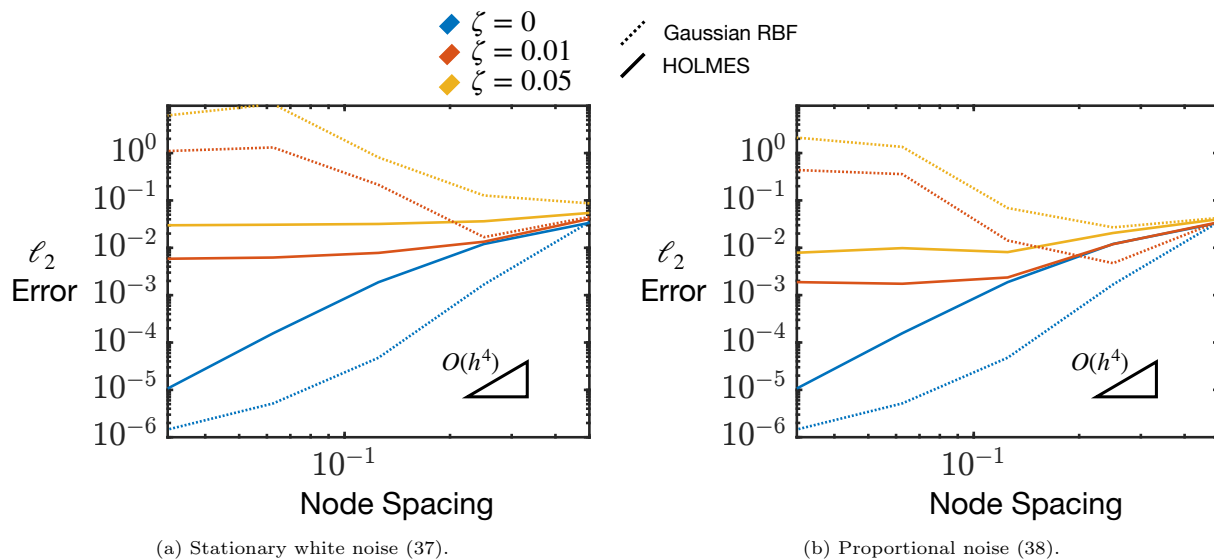


Figure 6: ℓ_2 error for a Gaussian hill function with varying noise amplitude as given by (37) and (38) using RBF-Gaussian interpolation (dotted lines) and the HOLMES approximants (solid lines). $\mathcal{O}(h^4)$ scaling shown with dot-dashed line. ζ correspond to the white noise amplitude used. HOLMES approximants computed using $\gamma \approx 0.8$ for a distance norm of $p = 2$.

Possibly the most popular RBF kernel is the Gaussian. Figure 6 compares the influence of noise on both RBF-Gaussian and HOLMES interpolation schemes, represented by dotted and solid lines respectively. The Gaussian RBF significantly outperforms HOLMES in the noiseless case of $\zeta = 0$ due to it being an exact interpolant rather than an approximant. Despite this, the addition of even 1% noise can have devastating effects on RBF accuracy. The convergence plots do not plateau at some level proportional to the noise magnitude, but explode and entirely ruin the interpolation. RBF-Gaussian is known to be highly sensitive to its kernel parameter [25], but even extensive manual manipulation could not achieve better results than HOLMES for this case, making it a poor choice for an interpolation scheme in the presence of noise.

An analysis of RBF performance would be amiss to neglect the popular family of Wendland kernels [26], whose compact support make them more computationally practical than the Gaussian kernel. Figure 7 summarizes this analysis, where vastly superior noise resistance is found compared to the RBF-Gaussian interpolation, but accuracy is still inferior to HOLMES interpolation. HOLMES and

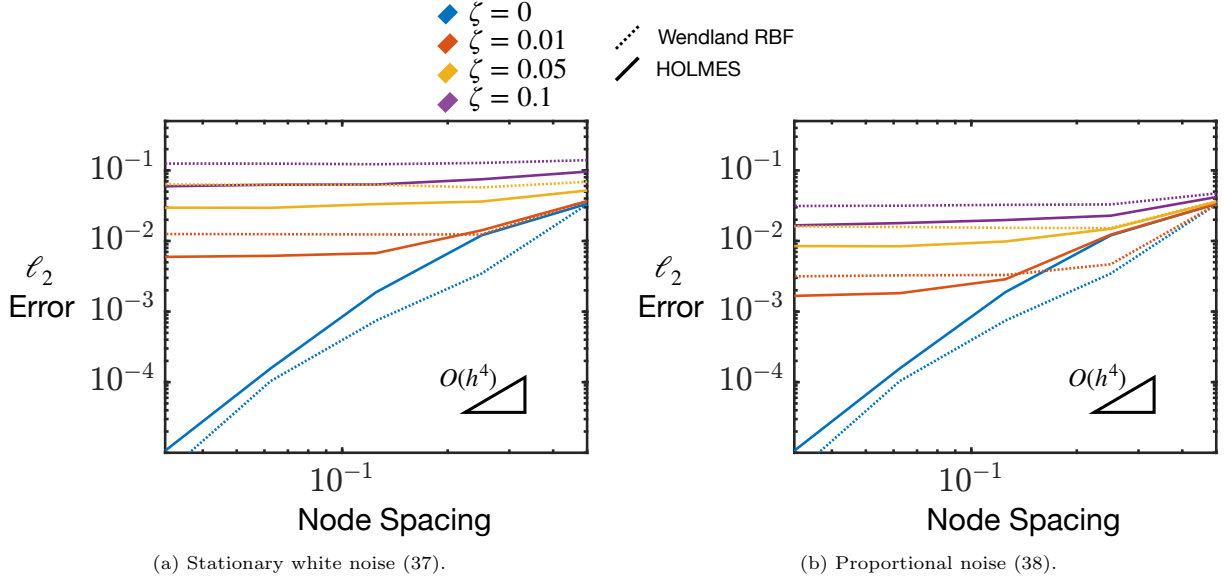


Figure 7: ℓ_2 error for a Gaussian hill function with varying noise amplitude as given by (37) and (38) using RBF-Wendland Interpolations (dotted lines) and the HOLMES approximants (solid lines). $O(h^4)$ scaling shown with dot-dashed line. σ correspond to the white noise amplitude used. HOLMES approximants computed using $\gamma \approx 0.8$ for a distance norm of $p = 2$.

RBF-Wendland are using identical cutoff radii in this analysis to make a more equal comparison, but the behaviour with noise is similar regardless of how large a cutoff radius RBF-Wendland is allowed. RBF-Wendland consistently plateaued at around 150% the error of HOLMES once noise was introduced. It should be noted that RBF-Wendland again performs better than HOLMES in the noiseless case because it is an exact interpolant, but this is the very reason it performs poorly with noise. RBF interpolation risks overfitting as it attempts to exactly replicate the known data points, whereas HOLMES relaxes this constraint in favour of maximizing entropy.

On the other hand, HOLMES is relatively insensitive to its locality parameter γ , which can generally be left at $\gamma \approx 0.8$ for a distance norm of $p = 2$ [38]. Since higher order distance norms cause faster shape function decay, and thus, fewer neighbours, this work has adjusted γ to maintain the same number regardless of norm used through $\gamma(p) = \gamma_0^{p/p_0} (-1 - \log(\epsilon))^{1-p/p_0}$, with $\gamma_0 = 0.8$, $p_0 = 2$, $\epsilon = 2e-16$. This scales γ to maintain the same neighbourhood, and takes $\gamma = 0.8$ and $p_0 = 2$ as a good standard.

RBF interpolants can be made more resistant to data noise making them approximants like HOLMES [19]. This approach is effective in many situations, but requires some indication of how to choose smoothing parameters. For the common case of unreplicated experiments this paper is concerned with, where few if any of the statistical features of the data are known, there is no reliable approach for parameter selection. If any approach is to be applied without manual intervention to increase resolution of computer simulations it becomes clear manual smoothing parameters will be *ad hoc* and unreliable.

4. Examples

This section deals with a variety of examples to demonstrate the basic functionality of the proposed DoE method and investigate its parameters. A comparison is made in subsection 4.3 to a comparable

method which demonstrates the increased resistance to noise of the entire DoE scheme. Section 4.4 then investigates a simple approach to apply the DoE technique to time dependent problems, which could have interesting future applications to the numerical solution of PDEs.

It should be noted that all investigations in this work use a coarse FF grid as the starting point for the adaptive DoE method to work from. In general, any spacing filling approach would be appropriate for the initial seeding of data points, with the the user ultimately selecting the method most appropriate to their specific problem. While it is evident that the initial seed will influence the result of the DoE method, the immense number of different seeding methods coupled with their performance on different types of problems makes a thorough investigation outside the scope of this work. A FF seed is chosen for these experiments because of its simplicity, not because it achieves the best results on any particular problem.

4.1. Canonical Functions

A successful DoE method should reproduce certain results on simple canonical functions. Specifically, the sampling of a radially symmetric function should be radially symmetric, and that of a plane function should be space filling. Initially, the proposed method could not achieve this because of non-existent HOLMES derivatives along the domain boundary [38], and large numerical errors in derivative evaluations very close to the boundary. A potential solution could use L'Hôpital's rule to evaluate the derivatives along the boundary [57], but would be non-trivial to implement in multiple dimensions. An easily implemented practical solution is to recognize that derivatives only suffer significant distortion very close to the boundary, and restrict the DoE method from considering points within this region. This could be problematic when the region of interest lies along a boundary, but otherwise does not severely handicap the technique.

Figure 8 demonstrates the approach after suitably restricting the sample point domain. The method now replicates the expected space-filling and radially symmetric results within the limit of the 41×41 evaluation grid.

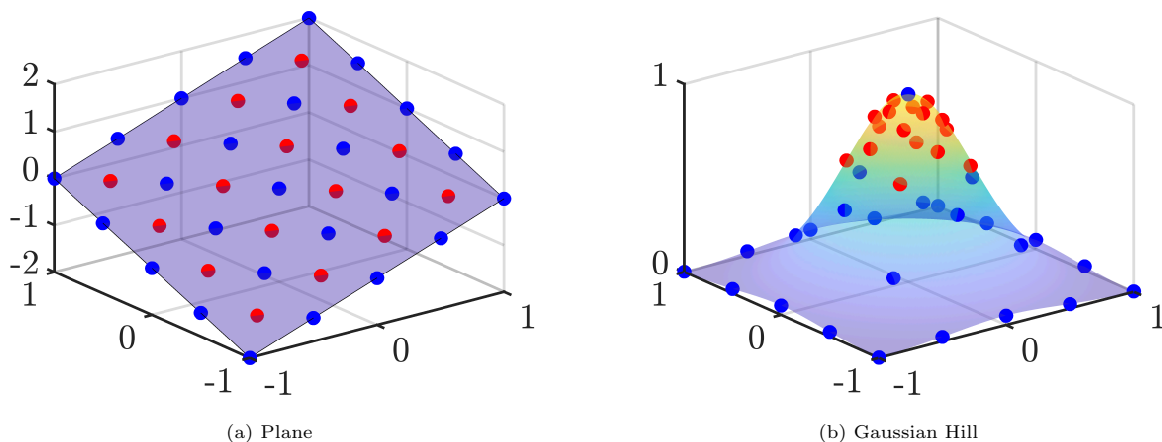


Figure 8: Adaptive DoE nodal distribution for two test functions (a) plane and (b) Gaussian Hill (see Appendix A). Initially, 25 points were selected using space filling distribution (red points). Additional 16 points (blue) were placed in the domain according to the DoE. The space filling and radial distribution location of points for the respective test functions are as expected. HOLMES approximants computed using $p = 3$, order 3, and $\gamma = 0.12$.

Performance of the adaptive method can be compared to the popular non-adaptive methods of LHS and full factorial design by constructing a separate HOLMES approximation with each distinct set of data points and comparing ℓ_2 errors over the domain $[-1, 1]^2$. The Gaussian hill is used and the underlying function in this test case, since the plane is perfectly approximated by HOLMES. In this case a 100×100 evaluation grid was used to calculate ℓ_2 error, all methods began with a 5×5 grid of data points, and HOLMES parameters of $p = 3$ and $\gamma = 0.12$ were used. Figure 9 shows the results. Error is seen to drop rapidly with a few targeted data point additions by the adaptive method, while the error of non-adaptive methods decreases in a slow, but steady manner. The initial samples are especially impressive, as they reduce the error by a factor of 5 with the addition of only 8 points to the starting set. Evidently, the main source of error occurs at the peak of the Gaussian, and once that is eliminated the smaller errors distributed throughout the domain will take longer to deal with. This concept is demonstrated on the right side of Figure 9, where the strategic addition of two points can massively improve a HOLMES interpolation in 1D. This example is particularly striking because the errors are concentrated in a small area, and thus quickly eliminated. The benefits of an adaptive DoE technique would not appear as striking for a function with a less concentrated error profile – nor would they be expected to be.

It should be noted that throughout this work, ℓ_2 error results provided by LHS are considered as the average of 100 tests to offset the intrinsic randomization of the technique. This number of samples provides a reasonable indication of the trajectory of the ℓ_2 error.

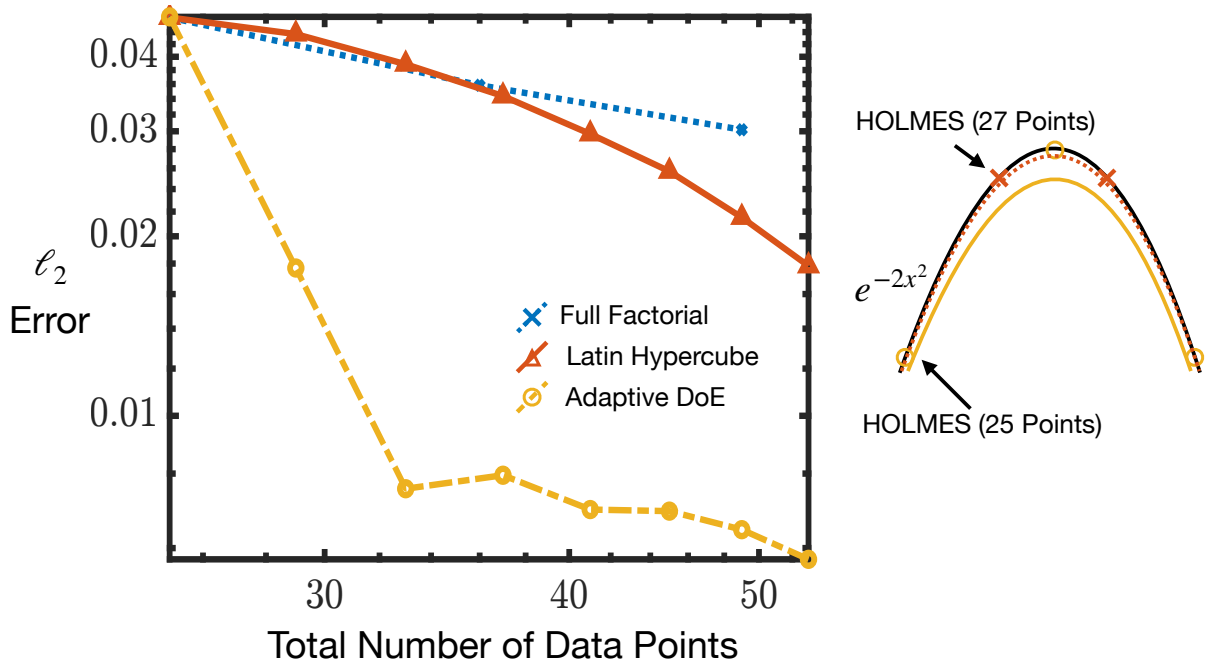


Figure 9: Comparison of the ℓ_2 error evolution with the number of data points between the proposed adaptive DoE (dot-dashed line), LH (solid line), and FF (dotted line) methods on a Gaussian hill test function (see Appendix A). The test function was evaluated using the metamodels on an evenly distributed 100×100 grid over the domain $[-1, 1]^2$. HOLMES approximants computed using $p = 3$, order 3, and $\gamma = 0.12$.

4.2. Influence of Kernel Parameter

The kernel parameter, ξ , used in the spacing function $h(x)$ has a large influence on the resulting point distribution, as mentioned in subsection 2.1.2. The choice of scalar, R_0 , which modifies ξ via (8) and (9), has a significant influence on the DoE method. Figure 10 demonstrates this with a log-scaled Rosenbrock function. Smaller values of R_0 will allow tighter clumping of points, since Q_S only becomes dominant very close to a data point. An extreme case of this can be found in figure 10a, where the data points are clearly far too concentrated. Larger values will enforce a spacing filling distribution with increasing severity as Q_S becomes dominant nearly everywhere.

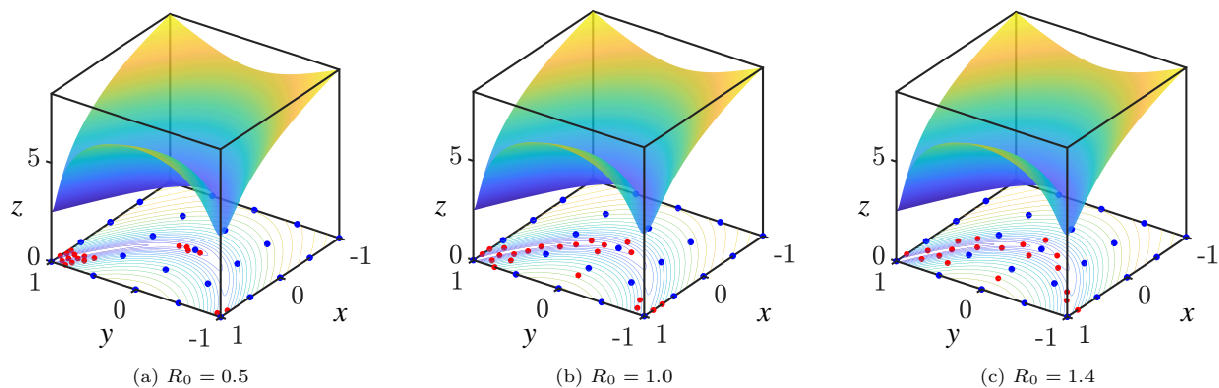


Figure 10: Log-scaled Rosenbrock function (see Appendix A) nodal distributions showing 25 initial points (blue) evenly distributed in the domain $[-1, 1]^2$. Additional 18 nodes were added using the adaptive DoE technique using different values of the kernel size, R_0 , to show the influence in the placement of these points. HOLMES approximants computed using $p = 3$, order 3, and $\gamma = 0.12$.

An investigation of this influence on accuracy is performed through comparison of the ℓ_2 error of the metamodel as a function of both the total number of samples and the value of R_0 . Figure 11 demonstrates the influence of this parameter when interpolating the Rosenbrock function above. The comparison was repeated for multiple test functions of varying linearity, all of which may be found in Appendix A.

Table 1 shows the ℓ_2 error after adding 0, 8 and 80 points to a 5×5 full factorial design through the DoE algorithm. The functions used are provided in Appendix A. Data for $R_0 = 0.5$ and $R_0 = 1.4$ are shown as a sample, though data on the range $R_0 = [0.25, 1.75]$ was collected.

In general, smaller values of R_0 work well when the underlying function has more localized extrema, but quickly result in a clumped samples which perform poorly in general. A larger value of R_0 naturally emphasizes more of the space-filling criteria, and thus, performs more consistently than small R_0 tests, but with fewer benefits over using a non-adaptive approach. This is why, for the functions in table 1, the $R_0 = 1.4$ designs generally, but not always perform better than the $R_0 = 0.5$ ones. Values in the range $R_0 = [1, 1.5]$ perform most consistently overall, which is consistent with the results of [17]. A value of 1.25 is used throughout the remainder of this work.

4.3. Influence of Error

Comparing the proposed method to LHS or any Monte Carlo-style simulation in the realm of robustness against noise is not especially helpful for assessing an adaptive DoE approach. Randomized simulations with an equal chance of choosing any point within the domain will naturally be the least

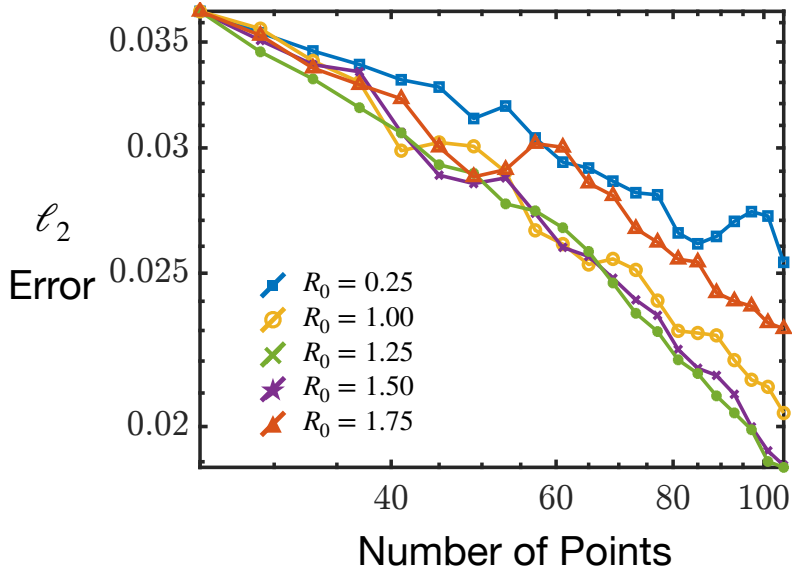


Figure 11: ℓ_2 error vs. number of data points for several values of $R_0 = [0.25, 1.4]$. The test function used in this test was the log-scaled Rosenbrock function (see Appendix A) evaluated on an evenly distributed 100×100 evaluation grid over the domain $[-1, 1]^2$. HOLMES approximants computed using $p = 3$, order 3, and $\gamma = 0.12$.

Function	$R_0 = 0.5$			$R_0 = 1.4$	
	0 Points	8 Points	80 Points	8 Points	80 Points
T1 Gaussian	4.66	1.56	0.30	0.76	0.01
T2 Rosenbrock	7.84	7.27	5.13	7.10	4.04
T3	9.32	8.80	1.54	6.91	0.63
T4	8.31	7.83	6.50	7.60	3.20
T5	34.93	29.77	15.42	32.79	11.71
T6	16.75	9.40	3.82	10.57	2.21
T7 Branin	1.44	1.38	0.60	1.47	0.57
T8 Himmelblau	8.78	7.615	2.70	7.48	1.95
T9 Rosenbrock	10.57	8.62	4.59	9.46	5.52

Table 1: ℓ_2 error (2) at 8 and 80 points for several test functions detailed in Appendix A. Designs produced with a spacing parameter of $R_0 = 0.5$ and $R_0 = 1.4$ are compared. HOLMES approximants computed using $p = 3$, order 3, and $\gamma = 0.12$.

statistically biased, and therefore the most robust against errors in the data. A better comparison for the DoE method in general is to a similar adaptive sampling method designed for unreplicated experiments.

An adaptive DoE method with the objective function given by $S(x) = Q_L Q_S$ was previously found to yield strong results on a number of test functions [17]. This objective function uses an identical spacing parameter, Q_S . The linearity criterion is also similar, but created using RBF interpolation with C2 Wendland functions rather than HOLMES functions. There is no LOO error criteria. The linearity criterion as originally provided was not normalized onto $[\epsilon, 1]$, but has been here to ensure more consistent performance than the original algorithm, which was found to perform erratically on most functions.

Let us again consider a plane function, but apply proportional Gaussian error to the collected data at each iteration. Both DoE algorithms are then run with $36 + 40 \times 4$ data points. Since subsection 3.3 demonstrated the superiority of HOLMES in direct interpolation with noise, it is not fair to compare the quality of data point placements using different interpolation methods for final error calculations. Instead, after all points are collected, the solution is interpolated via a separate interpolation scheme –

LME interpolants – and the ℓ_2 error is calculated on a 100×100 grid over the domain $[-1, 1]^2$. This ensures the quality of the DoE point placements is compared, and not just the final interpolation method. The results are seen in Figure 12. The difference between the two methods is insignificant for small amounts of error, but becomes very noticeable once a moderate amount of error is achieved. higherhigher

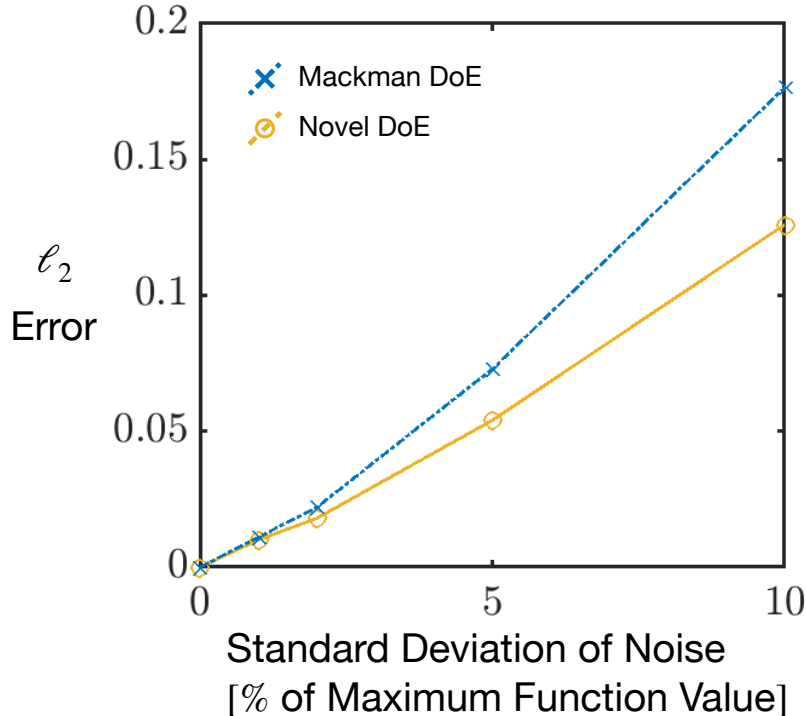


Figure 12: Comparison of Novel DoE and Mackman DoE with regards to robustness in data noise and $36 + 40 \times 4$ data points. ℓ_2 error in plane function interpolation is calculated with 100×100 points with different standard deviations of data point noise, measured as a percentage of the maximum function magnitude. HOLMES approximants computed using $p = 3$, order 3, and $\gamma = 0.12$. Both algorithms use a nodal spacing parameter $R_0 = 1.25$.

The improvement in accuracy does come at a computational cost. In the tests performed here, HOLMES functions generally evaluate slower than an equivalent RBF interpolation; however, RBF interpolation requires inverting a matrix whose size depends on the number of data points, while HOLMES interpolation scales instead with the number of points the metamodel is evaluated at. There could exist a situation in which this difference in scaling proves favourable for the HOLMES DoE. Nonetheless, in most cases custom shape functions like HOLMES come at a computational cost. This cost can be minimized or ignored if data collection is much slower than the DoE algorithm, or if computation of HOLMES shape functions can be smoothly integrated into a computer experiment itself. For example, by choosing HOLMES as the shape function in a scheme for solving PDEs – a topic which will be briefly considered in the next section.

4.4. Adaptive DoE for Time Dependent Functions

Time dependent functions are not generally considered as distinct from other functions in DoE methodology. Time may be considered a separate dimension in the design space, and points placed according to that. This approach makes sense in a non-adaptive method, since all points can be established prior to

the start of testing. For an adaptive method this cannot work, since the experimentalist cannot collect data from a time that has already passed.

The top-level approach taken here is very basic: known data points from previous times are projected to some point in the future, and the metamodel is constructed with these points. This projected metamodel is then used in the DoE approach as described above. New points are proposed, and these are used at the next timestep. In addition to a metamodel without any sort of projection, the approximation methods used are forward Euler (FE), where $u(x, t_{n+1}) \approx u(x, t_n) + \partial u / \partial t|_{t_n} \Delta t$, backward Euler (BE), where $u(x, t_{n+1}) \approx u(x, t_n) + \partial u / \partial t|_{t_{n+1}} \Delta t$, and explicit midpoint method (ME), where $u(x, t_{n+1}) \approx u(x, t_n) + \partial u / \partial t|_{t_{n+1/2}} \Delta t$ and $u(x, t_{n+1/2}) \approx u(x, t_n) + \partial u / \partial t|_{t_n} \Delta t / 2$. All derivatives with respect to t are estimated via a second order, three-point, backwards difference approximation when applicable, but since the recently added nodes did not necessarily exist in the past, their values are estimated based on previous metamodels, which are stored for this purpose.

Another important detail of the approach is the presence of a set of nodes arranged in a coarse full factorial grid which remains throughout all timesteps. In the simulations considered, a constant 5×5 grid of nodes will exist in every timestep, with the remaining 24 nodes added according to the DoE algorithm at each timestep. The results are compared to a full factorial design of 7×7 nodes.

The axisymmetric $2d$ wave equation,

$$u_{tt} = c^2 \left(\frac{1}{r} (ru_r)_r + \frac{1}{r^2} u_{\theta\theta} \right), \quad (39)$$

is chosen for investigating this approach. The solution will produce a smoothly time-evolving function, and is relevant to both physical and computer experiments. Specifically, the classical problem of vibration on an axisymmetric circular drum of radius $R = \sqrt{2}$ and constant $c = 1$ is chosen, resulting in boundary conditions of $u(R, t) = 0$ and regularity in the solution at $u(0, t)$. A Gaussian initial condition is selected as

$$u(r, 0) = U \left(e^{-\frac{\xi}{R^2} r^2} - e^{-\xi} \right). \quad (40)$$

The solution can be found via separation of variables as (41).

$$u(r, t) = \sum_{n=1}^{\infty} A_n \cos(c\lambda_{0n}t) J_0(\lambda_{0n}r), \quad (41)$$

where $\lambda_{0n} = z_{0n}/R$, and z_{0n} is the n^{th} zero of the Bessel function of the first kind, $J_0(z)$. The coefficients, A_n , are determined via orthogonality. The summation requires 33 terms to match the initial condition in (40) to computer precision.

For convenience, the resulting metamodel accuracy is evaluated on an evenly spaced 100×100 grid of points covering $[-1, 1]^2$. The nature of the problem investigated results in error norms which oscillate in time, as in 13, so direct comparison between methods becomes difficult, other than to note the DoE methods seem to provide modest, though visible increases in accuracy over the full factorial design regardless of the method used to project node values through time.

A quantitative comparison is easier if the error is treated as an integrable function in time, and integration is performed numerically. In this case, trapezoidal rule is used over a simulation time of 20s.

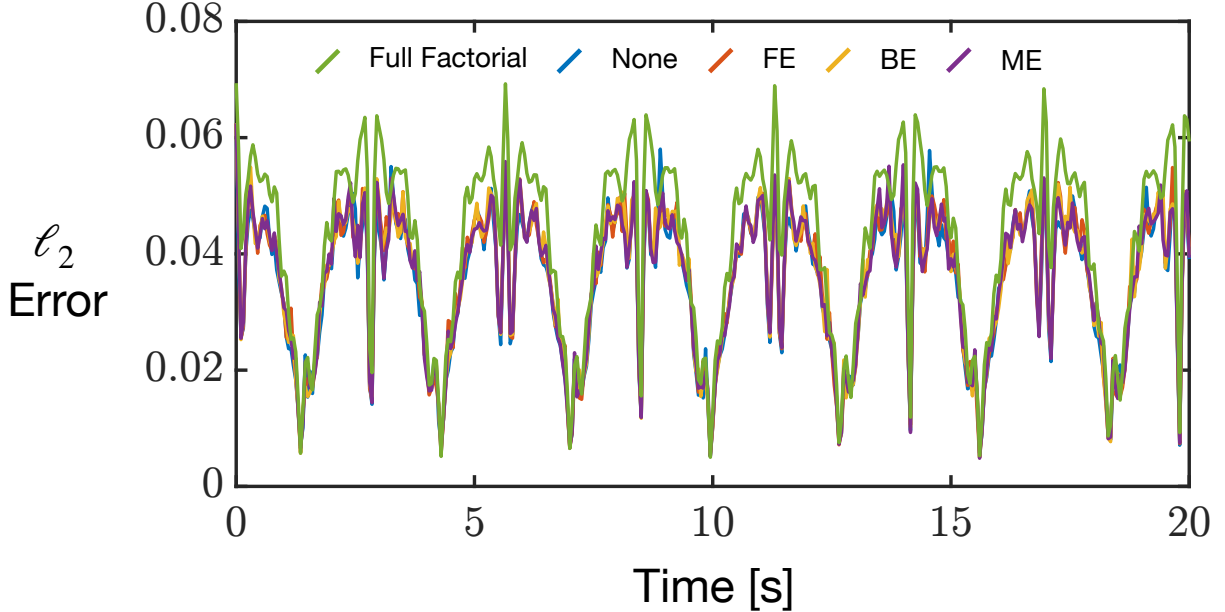


Figure 13: Discrete ℓ_2 error in metamodel as a function of time over $[-1, 1]^2$ with 50×50 sample points. HOLMES approximants computed using $p = 3$, order 3, and $\gamma = 0.12$. DoE methods used are as follows: (a). Constant full factorial design (FF), and adaptive DoE algorithm with nodes projected into the future using (b). No projection (None), (c). Forward Euler (FE), (d). Backward Euler (BE), and (e). Explicit Midpoint method (ME).

The results in 14 conform to expectations. Namely, some reasonable increase in accuracy is generally achieved by the DoE methods compared to the full factorial approach. The increase is around 10 – 15% when DoE method is allowed to update the node positions frequently, but decreases as node placements become less frequent. For long update times, the difference between DoE and full factorial performance becomes insignificant.

The projection of DoE nodes in the metamodel does have some effect in mitigating the influence of less frequent node placements. Un-projected nodes result in a DoE method which is most sensitive in this regard, while all the projected methods appear to be more robust. Performance of all methods becomes worse with decreased DoE placement frequency.

The approach described in this section is simple, and has some obvious limitations. It only makes sense to project data points a small time into the future, and clearly the efficacy of the resulting DoE is dependent on the accuracy of the approximation. The allowable timestep will depend on the experiment at hand, and the experimentalist will likely require some *a priori* knowledge of the timescale of their problem. In the above example, knowledge of the analytical solution was used to approximately set a suitable timestep, and the results were satisfactory without additional effort.

The density of the initial full factorial grid could also be examined in detail. Would a larger proportion of points added through the adaptive DoE method be beneficial, or detrimental? No attempt is made to investigate this beyond noting that, for the arbitrary combination of full factorial and DoE points chosen, there was some improvement without any attempt at tuning, which could hint at some robustness in the approach.

Additionally, in a physical experiment the experimentalist must have time to both run the DoE algorithm, and adjust any measurement devices to capture the recommended data points, within the time

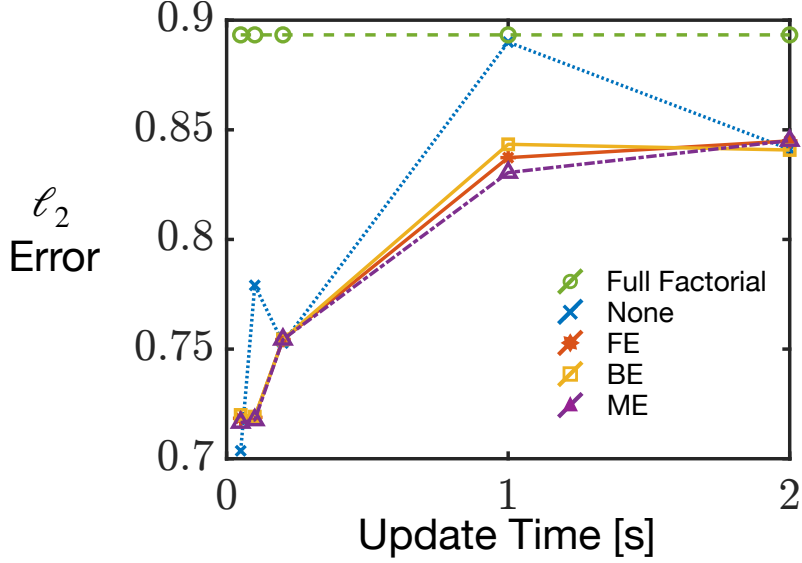


Figure 14: Discrete ℓ_2 error in metamodel as measured over $[-1, 1]^2$ with 50×50 sample points integrated over the time interval $[0, 20]$ s vs DoE update interval. HOLMES approximants computed using $p = 3$, order 3, and $\gamma = 0.12$. DoE methods used are as follows: (a). Constant full factorial design (FF), and adaptive DoE algorithm with nodes projected into the future using (b). No projection (None), (c). Forward Euler (FE), (d). Backward Euler (BE), and (e). Explicit Midpoint method (ME).

constraints posed by the forward projection of data points. It would be unsurprising if such conditions could not be met in the vast majority of physical experiments; however, computer experiments would be much more likely to benefit from such an approach. A time-dependent computer experiment could be periodically paused for the insertion of additional points, and resumed as needed – just as is done in the above example, but where the additional points are used in the experimental calculations. This exploration is out of scope of the current work, but it is possible that particle-based continuum mechanics simulations, such as smoothed particle hydrodynamics, could benefit from such an approach. Errors will accumulate through time in such simulations, so the cumulative effect of even modest increases in accuracy can be significant by the end of a simulation.

5. Conclusion

We proposed a novel adaptive DoE method that balances curvature, space filling, and metamodel error considerations to automatically select nodes with an optimal location in the domain and approximate non-linear functions within the design space. HOLMES with a variable kernel size is introduced to satisfy the adaptive nature of the proposed method. Adaptive HOLMES metamodeling provides accurate function and derivative approximations on the interior of the domain, making it more suitable for handling data with moderate Gaussian white noise than schemes using radial basis functions. The key parameter of the method, R_0 , was investigated and can generally be set within a limited range. Additionally, we proposed alternative ways to estimate the local nodal spacing in unstructured data using the boundary-corrected KDE method.

Evaluation of the new method indicated better performance than simple, established, nonadaptive methods such as LH and FF on a set of test functions. Then method outperforms a similar adaptive

DoE method when noise is introduced into the simulation. Additionally, the approach becomes more applicable to time-dependent experiments when the metamodels were first projected forward in time.

Future work could adapt the proposed approach to the solution of partial differential equations. Specifically, this approach's unstructured, multidimensional nature could lend itself to particle-based continuum mechanics models, such as smoothed particle hydrodynamics, which are still developing strategies for dynamically and methodically increasing resolution during the simulation.

6. Acknowledgment

We acknowledge the support from the Natural Sciences and Engineering Research Council of Canada (NSERC) through the Discovery Grant under Award Application number 2016-06114 and the Alliance grant number AWD-014405. L.C. acknowledges the financial support from NSERC CGS M fellowship. This research partially was supported through computational resources and services provided by Advanced Research Computing at the University of British Columbia and Compute Canada.

Appendix A. Test Functions

The analytical test functions used were as follows. All were normalized onto $[-1, 1] \times [-1, 1]$. To compare ℓ_2 norm values between functions, all functions are also scaled by a constant A such that $\max_{x \in [-1, 1]^2} |f(x)| = 1$.

T0 Plane: $f(x, y) = x + y$,
 $x, y \in [-1, 1]$.

T1 Gaussian Hill: $f(x, y) = e^{-3(x^2+y^2)}$,
 $x, y \in [-1, 1]$.

T2 Log-Scaled Rosenbrock: $f(x, y) = \log(1 + (100(y - x^2)^2 + (1 - x)^2))$,
 $x, y \in [-1, 1]$.

T3 $f(x, y) = 2 + 0.01(y - x^2)^2 + (1 - x)^2 + 2(2 - y)^2 + 7 \sin(0.5x) \sin(0.7xy)$,
 $x, y \in [0, 5]$.

T4 $f(x, y) = \cos(6(x - \frac{1}{2})) + 3.1(|x - 0.7|) + 2(x - \frac{1}{2}) + \sin\left(\frac{1}{|x - \frac{1}{2}| + 0.31}\right) + \frac{y}{2}$,
 $x, y \in [0, 1]$.

T5 $f(x, y) = \cos((x^2 + y^2)^{1/2})$,
 $x, y \in [-5, 5]$.

T6 $f(x, y) = \sin(x) \sin(y)$, $x, y \in [-3, 3]$.

T7 Branin's Function: $f(x, y) = \left(y - 5.1 \left(\frac{x}{2\pi}\right)^2 + \frac{5x}{\pi} - 6\right)^2 + 10 \left(1 - \frac{\pi}{8}\right) \cos(x) + 10$,
 $x \in [0, 15]$, $y \in [-5, 10]$

T8 Himmelblau's Function: $f(x, y) = (x^2 + y - 11)^2 + (x + y^2 - 7)^2$,
 $x, y \in [-4, 4]$.

T9 Rastrigin's Function: $f(x, y) = 20 + x^2 + y^2 - 10(\cos(2\pi x) + \cos(2\pi y))$,
 $x, y \in [-1, 1]$.

References

- [1] Luc Pronzato and Andrej Pázman. Design of Experiments in Nonlinear Models, volume 212. Springer Science+Business Media New York, 2013.
- [2] Ruichen Jin, Wei Chen, and Agus Sudjianto. On Sequential Sampling for Global Metamodeling in Engineering Design. In ASME 2002 Design Engineering Technical Conferences and Computers and Information in Engineering Conference, pages 1–10, 2002.
- [3] M. D. McKay, R. J. Beckman, and W. J. Conover. A comparison of three methods for selecting values of input variables in the analysis of output from a computer code. Technometrics, 21(2):239–245, 1979.
- [4] Art B. Owen. Orthogonal Arrays for Computer Experiments, Integration and Visualization. Statistica Sinica, 2(2):439–452, 1992.
- [5] Wynn H.P. Shewry M.C. Maximum entropy sampling. Journal of Applied Statistics, 14(2):165–170, 1987.
- [6] Chun-Wa Ko, Jon Lee, and Maurice Queyranne. An Exact Algorithm for Maximum Entropy Sampling. Operations Research, 43(4):684–691, 1995.
- [7] Frank O. Merkle. Constrained Maximum-Entropy Sampling. Operations Research, 46(5):655–664, 1998.
- [8] T. Guest and A. Curtis. Iteratively constructive sequential design of experiments and surveys with nonlinear parameter-data relationships. Journal of Geophysical Research: Solid Earth, 114(4):1–14, 2009.
- [9] Yu Wang, Nhu D. Le, and James V. Zidek. Approximately optimal subset selection for statistical design and modelling. Journal of Statistical Computation and Simulation, 2021.
- [10] M. Hamada, H. F. Martz, C. S. Reese, and A. G. Wilson. Finding near-optimal Bayesian experimental designs via Genetic algorithms. American Statistician, 55(3):175–181, 2001.
- [11] Raj K. Velicheti, Amber Srivastava, and Srinivasa M. Salapaka. Design of Experiments with Imputable Feature Data: An Entropy-Based Approach. preprint, 2021.
- [12] Paul Diaz, Alireza Doostan, and Jerrad Hampton. Sparse polynomial chaos expansions via compressed sensing and D-optimal design. Computer Methods in Applied Mechanics and Engineering, 336:640–666, 2018.
- [13] Jing Yu, Victor M. Zavala, and Mihai Anitescu. A scalable design of experiments framework for optimal sensor placement. Journal of Process Control, 67:44–55, 2018.

- [14] R. Ibañez, E. Abisset-Chavanne, E. Cueto, A. Ammar, J. L. Duval, and F. Chinesta. Some applications of compressed sensing in computational mechanics: model order reduction, manifold learning, data-driven applications and nonlinear dimensionality reduction. Computational Mechanics, 64(5):1259–1271, 2019.
- [15] Luc Pronzato and Werner G. Müller. Design of computer experiments: Space filling and beyond. Statistics and Computing, 22(3):681–701, 2012.
- [16] Noha Youssef and Henry Wynn. A discussion on adaptive designs for computer experiments. Sequential Analysis, 38(3):400–410, 2019.
- [17] T.J. Mackman and C.B. Allen. Investigation of an adaptive sampling method for data interpolation using radial basis functions. International Journal for Numerical Methods in Engineering, 83:915–938, 2010.
- [18] Genzi Li, Vikrant Aute, and Shapour Azarm. An accumulative error based adaptive design of experiments for offline metamodeling. Structural and Multidisciplinary Optimization, 40(1-6):137–155, 2010.
- [19] R. Theunissen and P. Gjelstrup. Adaptive sampling in higher dimensions for point-wise experimental measurement techniques. Measurement Science and Technology, 29(8), 2018.
- [20] Dario Azzimonti, David Ginsbourger, Clément Chevalier, Julien Bect, and Yann Richet. Adaptive Design of Experiments for Conservative Estimation of Excursion Sets. Technometrics, 63(1):13–26, 2021.
- [21] Zhanglin Li, Xialin Zhang, Keith C. Clarke, Gang Liu, and Rui Zhu. An automatic variogram modeling method with high reliability fitness and estimates. Computers and Geosciences, 120(August):48–59, 2018.
- [22] Aikaterini P. Kyprioti, Jize Zhang, and Alexandros A. Taflanidis. Adaptive design of experiments for global Kriging metamodeling through cross-validation information. Structural and Multidisciplinary Optimization, pages 1135–1157, 2020.
- [23] Hiromasa Kaneko. Adaptive design of experiments based on Gaussian mixture regression. Chemometrics and Intelligent Laboratory Systems, 208(November 2020):104226, 2021.
- [24] Andrea Da Ronch, Marco Panzeri, M. Anas Abd Bari, Roberto D’Ippolito, and Matteo Franciolini. Adaptive design of experiments for efficient and accurate estimation of aerodynamic loads. Aircraft Engineering and Aerospace Technology, 89(4):558–569, 2017.
- [25] M.D. (University of Giessen) Buhmann. Radial Basis Functions. Cambridge University Press, Cambridge, UK, 2003.
- [26] Holger Wendland. Scattered Data Approximation. Cambridge University Press, New York, 2005.

- [27] Timothy J. Barth, Michael Griebel, David E. Keyes, Risto M. Nieminen, Dirk Roose, and Tamar Schlick, editors. 27th International Meshing Roundtable. Springer Nature Switzerland, 2019.
- [28] Zhiliang Liu, Ming J. Zuo, Xiaomin Zhao, and Hongbing Xu. An analytical approach to fast parameter selection of gaussian RBF kernel for support vector machine. Journal of Information Science and Engineering, 31(2):691–710, 2015.
- [29] Victor Picheny, David Ginsbourger, Olivier Roustant, Raphael T. Haftka, and Nam Ho Kim. Adaptive designs of experiments for accurate approximation of a target region. Journal of Mechanical Design, Transactions of the ASME, 132(7):0710081–0710089, 2010.
- [30] Marino Arroyo and M. Ortiz. Local maximum-entropy approximation schemes: A seamless bridge between finite elements and meshfree methods. International Journal for Numerical Methods in Engineering, 65(13):2167–2202, 2006.
- [31] Bo Li. The Optimal Transportation Method in Solid Mechanics. PhD thesis, California Institute of Technology, 2009.
- [32] F Habbal. The Optimal Transportation Meshfree Method for General Fluid Flows and Strongly Coupled Fluid-Structure Interaction Problems. PhD thesis, California Institute of Technology, 2009.
- [33] Mathieu Foca. On a Local Maximum Entropy interpolation approach for Simulation of Coupled Thermo-mechanical Problems. PhD thesis, Ecole Centrale de Nantes, 2015.
- [34] HAO Jiang. A Micromechanical Computational Framework for Dynamic Failure Mechanisms in Polycrystalline Materials. PhD thesis, Case Western Reserve University, 2019.
- [35] Hao Wang, Huming Liao, Zongyue Fan, Jiang Fan, Laurent Stainier, Xiaobai Li, and Bo Li. The Hot Optimal Transportation Meshfree (HOTM) method for materials under extreme dynamic thermomechanical conditions. Computer Methods in Applied Mechanics and Engineering, 364, 2020.
- [36] C.J. Cyron, M. Arroyo, and M. Ortiz. Smooth, second order, non-negative meshfree approximants selected by maximum entropy. International Journal for Numerical Methods in Engineering, 79(February):1605–1632, 2009.
- [37] David Gonzalez and Ehas Cueto, Manuel Doblare, and Aragon Institute of Engineering Research. A higher order method based on local maximum entropy approximation. Proceedings of the 2011 American Control Conference, 83:741–764, 2010.
- [38] A. Bompadre, L. E. Perotti, C. J. Cyron, and M. Ortiz. Convergent meshfree approximation schemes of arbitrary order and smoothness. Computer Methods in Applied Mechanics and Engineering, 221-222:83–103, 2012.
- [39] Mustafa Murat Arat and Serpil Aktaş. Generalized maximum entropy approach to unreplicated factorial experiments. Statistics and its Interface, 9(3):295–302, 2016.

- [40] Kutz J.N. Brunton S.L. Data-Driven Science and Engineering. Cambridge University Press, 2019.
- [41] D. Bingham, A. Dean, M. Morris, and J. Stufken. Handbook of Design and Analysis of Experiments. Chapman and Hall/CRC, 1 edition, June 2015.
- [42] Annette M. Molinaro, Richard Simon, and Ruth M. Pfeiffer. Prediction error estimation: A comparison of resampling methods. Bioinformatics, 21(15):3301–3307, 2005.
- [43] N Sukumar. Construction of polygonal interpolants : a maximum entropy approach. International Journal for Numerical Methods in Engineering, 61:2159–2181, 2004.
- [44] Roman A. Polyak. Regularized Newton method for unconstrained convex optimization. Mathematical Programming, 120(1 SPEC. ISS.):125–145, 2009.
- [45] Pedro Navas, Susana López-Querol, Rena C. Yu, and Manuel Pastor. Optimal transportation mesh-free method in geotechnical engineering problems under large deformation regime. International Journal for Numerical Methods in Engineering, 115(10):1217–1240, 2018.
- [46] Jiang Fan, Huming Liao, Renjie Ke, Erdem Kucukal, Umut A. Gurkan, Xiuli Shen, Jian Lu, and Bo Li. A monolithic Lagrangian meshfree scheme for Fluid–Structure Interaction problems within the OTM framework. Computer Methods in Applied Mechanics and Engineering, 337:198–219, 2018.
- [47] A. Rosolen, D. Millan, and M. Arroyo. On the optimum support size in meshfree methods: A variational adaptivity approach with maximum-entropy approximants. Int. J. Numer. Meth. Engng, 1(February):82:868–895, 2010.
- [48] M. Rosenblatt. Remarks on Some Nonparametric Estimates of a Density Function. Annals of Mathematical Statistics, 27:832–837, 1956.
- [49] B.W. Silverman. Density Estimation for Statistics and Data Analysis. Chapman & Hall, London, 1998.
- [50] M. B. Liu and G. R. Liu. Smoothed particle hydrodynamics (SPH): An overview and recent developments. Archives of Computational Methods in Engineering, 17:25–76, 2010.
- [51] V. A. Epanechnikov. Non-Parametric Estimation of a Multivariate Probability Density. Theory of Probability and its Applications, 14(1):153–158, 1969.
- [52] J. Rice. Boundary modification for kernel regression. Communications in Statistics, Part A Theory and Methods, 13:893–900, 1984.
- [53] Peter Hall and Thomas E. Wehrly. A geometrical method for removing edge effects from kernel-type nonparametric regression estimators. Journal of the American Statistical Association, 86(415):665–672, 1991.
- [54] J.S. Marron and D. Ruppert. Transformations to Reduce Boundary Bias in Kernel Density Estimation. Journal of the Royal Statistical Society, 56(4):653–671, 1994.

- [55] Ashis Kumar Chakraborty and Moutushi Chatterjee. On multivariate folded normal distribution. Sankhya: The Indian Journal of Statistics, 75-B(1):1–15, 2013.
- [56] C.E. Shannon. A Mathematical Theory of Communication. Mobile Computing and Communications Review, 5(1), 1948.
- [57] F. Greco and N. Sukumar. Derivatives of maximum-entropy basis functions on the boundary: Theory and computations. International Journal for Numerical Methods in Engineering, 94(February):1102–1119, 2012.